-

Micrometeoroid and Orbital Debris Threat Assessment: Mars Sample Return Earth Entry Vehicle

Human Exploration Science Office/KX

[redacted]

September 2011

National Aeronautics and
Space Administration
Lyndon B. Johnson Space Center
Houston, Texas

Micrometeoroid and Orbital Debris Threat Assessment: Mars Sample Return Earth Entry Vehicle

Human Exploration Science Office/KX

Book Manager: James L. Hyde/ESCG
Senior Research Engineer, Hypervelocity Impact Technology Group

Environments & Analysis: Dr. Michael D. Bjorkman/ESCG
Senior Research Scientist, Hypervelocity Impact Technology Group

Modeling & Analysis: Kevin D. Hoffman/ESCG
Engineer, Hypervelocity Impact Technology Group

Concurrence: Dr. Eric L. Christiansen/NASA-JSC
Chief Analyst, Hypervelocity Impact Technology Group

Concurrence: Dana M. Lear/NASA-JSC
Analyst, Hypervelocity Impact Technology Group

Concurrence: Thomas G. Prior/ESCG
Project Manager, Hypervelocity Impact Technology Group

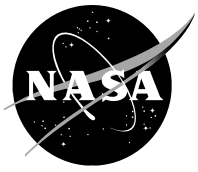

National Aeronautics and
Space Administration
Lyndon B. Johnson Space Center
Houston, Texas

Change Log

Rev	Date	Pages	Description
---	9/30/2011		Original Issuance

Table of Contents

Figures

Tables

Acronyms and Abbreviations

Al	aluminum
BUMPER	software application used for spacecraft MMOD risk assessments
BLE	Ballistic Limit Equation
EEV	Earth Entry Vehicle
EID	Element Identification Number (unique identification number)
ESCG	Engineering Services Contract Group
FEM	Finite Element Model
HITF	Hypervelocity Impact Technology Facility
HVI	Hypervelocity Impact
HVIT	Hypervelocity Impact Technology Group
I-DEAS	Integrated Design, Engineering, Analysis, and Simulation software
ISS	International Space Station
JSC	Johnson Space Center
MEM	Meteoroid Environment Model
MLI	Multi-Layer Insulation
MMOD	Micro-meteoroid Orbital Debris
MSR	Mars Sample Return
NASA	National Aeronautics and Space Administration
ORDEM2000	Orbital Debris Environment Model 2000
PID	Property Identification Number (used to index an element to a specific BLE)
PNP	Probability of No Penetration
PRA	Probabilistic Risk Assessment
TPS	Thermal Protection System
WSTF	White Sands Test Facility

1. Introduction

This report provides results of a Micrometeoroid and Orbital Debris (MMOD) risk assessment of the Mars Sample Return Earth Entry Vehicle (MSR EEV). The assessment was performed using standard risk assessment methodology illustrated in Figure 1-1. Central to the process is the Bumper risk assessment code (Figure 1-2), which calculates the critical penetration risk based on geometry, shielding configurations and flight parameters.

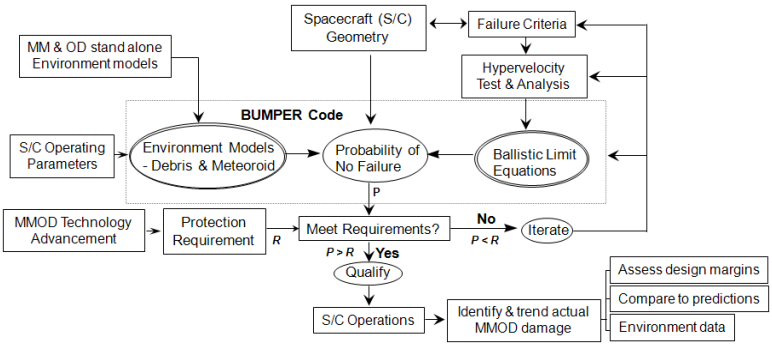

Figure 1-1. MMOD Risk Assessment Flowchart

The assessment process begins by building a finite element model (FEM) of the spacecraft, which defines the size and shape of the spacecraft as well as the locations of the various shielding configurations. This model is built using the NX I-deas software package from Siemens PLM Software. The FEM is constructed using triangular and quadrilateral elements that define the outer shell of the spacecraft. Bumper-II uses the model file to determine the geometry of the spacecraft for the analysis.

The next step of the process is to identify the ballistic limit characteristics for the various shield types. These ballistic limits define the critical size particle that will penetrate a shield at a given impact angle and impact velocity. When the finite element model is built, each individual element is assigned a property identifier (PID) to act as an index for its shielding properties. Using the ballistic limit equations (BLEs) built into the Bumper-II code, the shield characteristics are defined for each and every PID in the model.

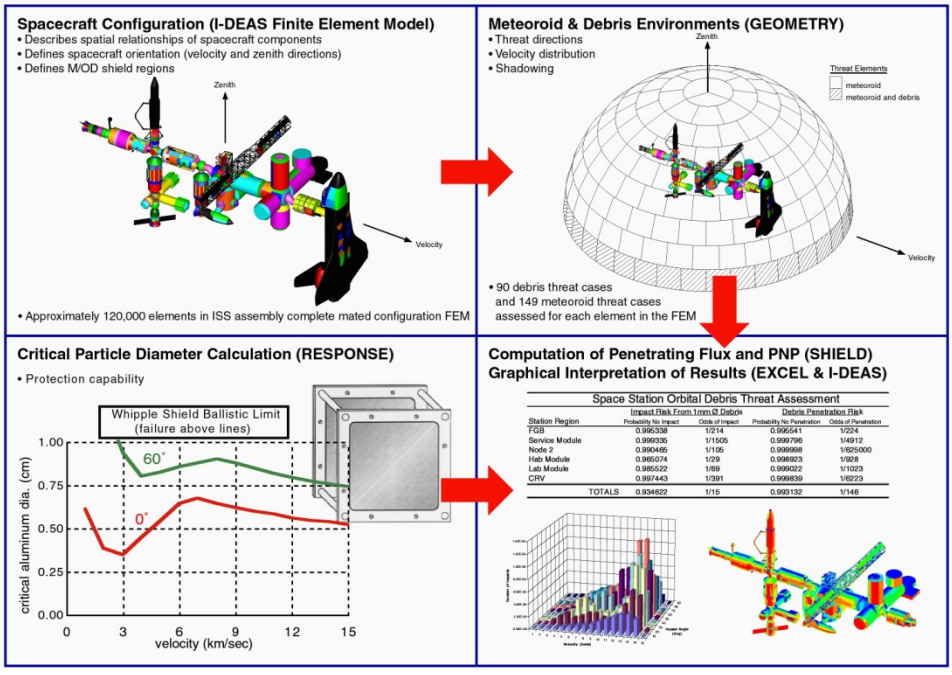

Figure 1-2. BUMPER-II MMOD Risk Assessment Code

The final stage of the analysis is to determine the probability of no penetration (PNP) on the spacecraft. This is done using the micrometeoroid and orbital debris environment definitions that are built into the Bumper-II code. These engineering models take into account orbit inclination, altitude, attitude and analysis date in order to predict an impacting particle flux on the spacecraft. Using the geometry and shielding characteristics previously defined for the spacecraft and combining that information with the environment model calculations, the Bumper-II code calculates a probability of no penetration for the spacecraft.

This report is prepared for NASA Ames Research Center (POC: Ethiraj Venkatapathy), and responds to a statement of work that is provided in Appendix A – MSR EEV MMOD Impact Risk Analysis Statement of Work.

2. Requirements

The results of this analysis were compared with a probability of containment not assured due to MMOD impact of 4.0×10^{-7}. This value was assigned during the August 9, 2011, monthly status teleconference. Project engineers made the allocation from the probabilistic risk assessment (PRA) fault tree (Gershman et al. 2005), reproduced below as Figure 2-1. MMOD impacts of the EEV can only result in a fault through the "EEV fails during correctly targeted entry" branch of the tree. Therefore, an allocation 4.0×10^{-7} to MMOD impact leaves nothing for other modes of failure during entry. Thus, unless a future reliability analysis shows that there are no other modes of failure occurring in this branch, the 4.0×10^{-7} probability should be taken as an upper bound on the requirement.

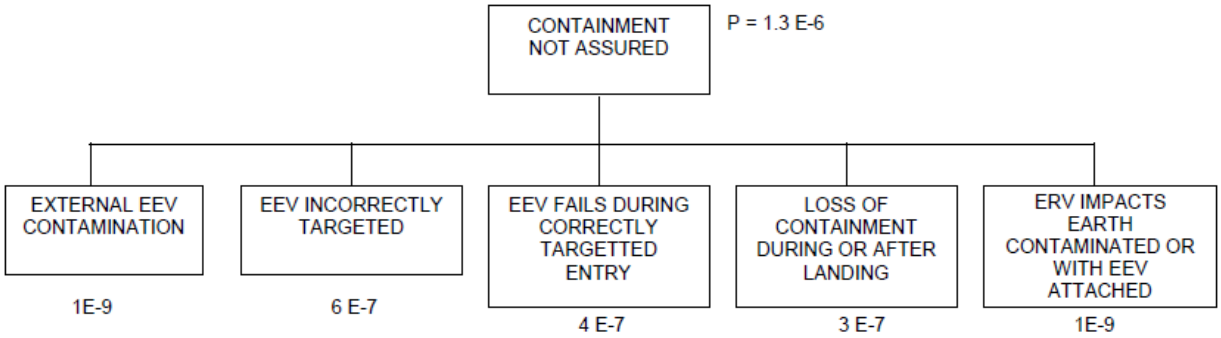

Figure 2-1. MSR EEV - PRA Fault Tree.

3. MSR EEV Thermal Protection System Design

The May 10, 2000 design for the MSR EEV is shown in cross section in Figure 3-1. The EEV is designed to land without parachutes, for maximum reliability. The blunt shape slows the EEV to a terminal speed of 41 m/s (92 mph) and the Earth impact loads are taken up by the spherical crushable structure. The orbital sample container is visible Figure 3-1 at the center the energy-absorbing sphere, which is composed of carbon foam plus webs. The blunt heat shield is a thin carbon-carbon structure; filled with carbon foam at the center and void at the circumference.

The current MSR EEV thermal protection system (TPS) has two parts. The forward TPS consists of 12mm of fully dense carbon phenolic. Carbon phenolic was selected for high reliability because of the extensive flight heritage and constitutes 1/3 of the total mass of the EEV. The aft TPS material has not been selected yet. Weight estimates were made with 10 mm of SLA-561V, and that is what is used in the MMOD impact risk assessment. Multilayer thermal insulation covers the MSR EEV's forward TPS and a portion of the aft TPS.

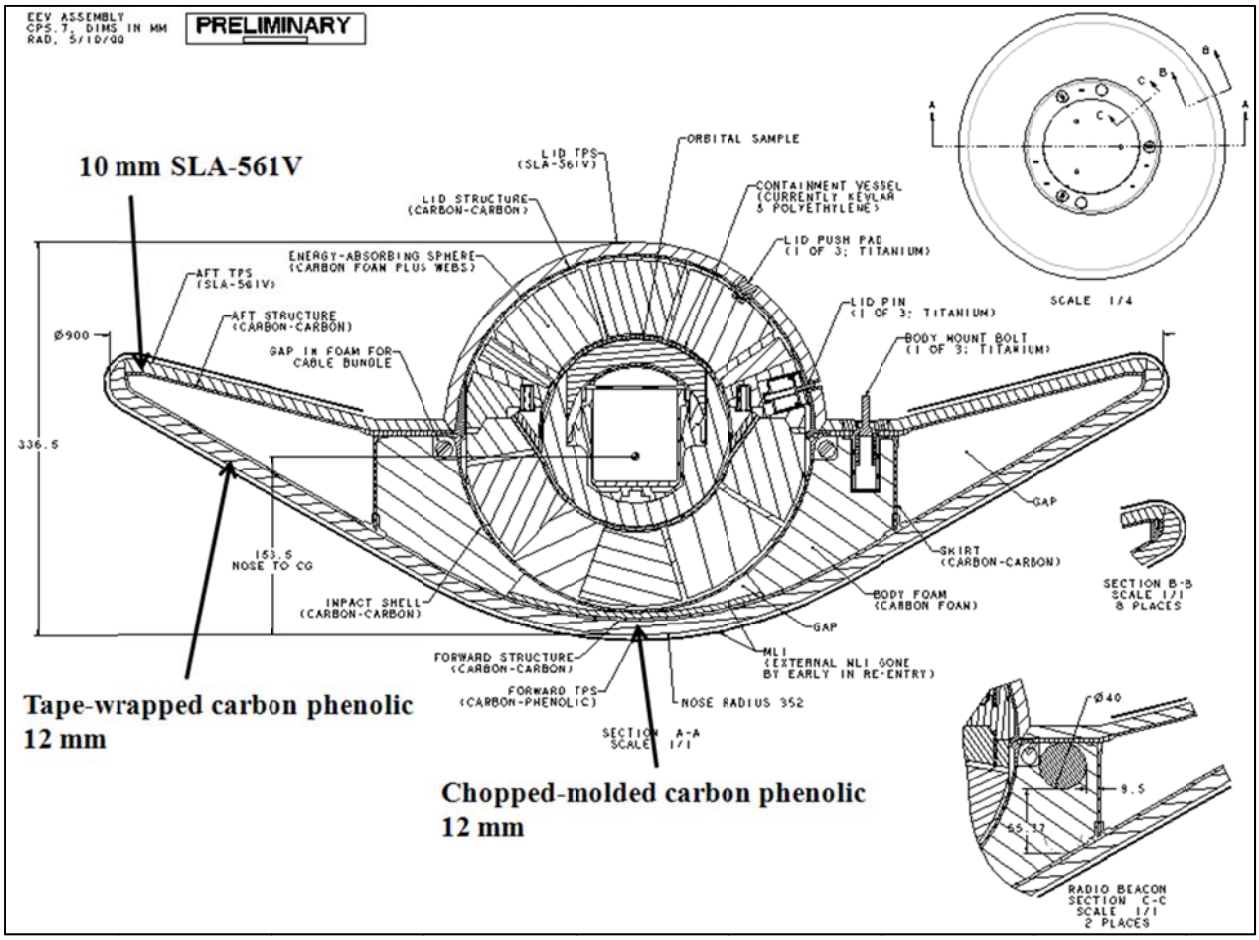

Figure 3-1. MSR EEV Shield Configuration.

4. Analysis

This section provides details on the analysis procedure and the Bumper-II input parameters used in the MSR EEV analysis.

4.1 Failure Criteria

Failure was defined as a perforation of the TPS down to the underlying structure. This failure criterion corresponds to a perforation through the 10 mm SLA-561V aft TPS or a perforation through the 12 mm carbon phenolic forward TPS.

These criteria are less conservative than what are used to evaluate the Orion MPCV. Penetration of no more than 25% to 80% of the Orion heat shield TPS thickness is allowable, depending on the location, and no more than 62% to 90% of the back shell TPS (Bohl, 2011). If the more conservative Orion TPS failure criteria apply to EEV, then the risk of containment not assured was underestimated in this report. Further work is recommended to confirm or change the EEV TPS failure criteria.

4.2 Configuration

Robert Maddox provided an EEV CAD model to JSC/KX engineers on April 14, 2011. A rendering of the CAD model is shown in Figure 4-1.

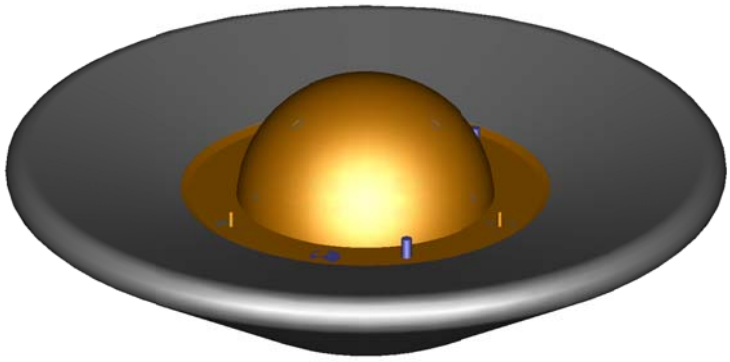

Figure 4-1. MSR EEV CAD Model.

Kevin Hoffman created the shell finite element models from the EEV CAD model for the MMOD analyses. Two components of the EEV were modeled: the forward and aft TPS systems. These two systems were divided into a total of 13 distinctive regions based on the structure below the TPS. Figure 4-2 is a rendering of the EEV FEM with the 13 regions colored and labeled. Dividing the model into regions permits the assignment of unique failure criteria to each region. Should further test and analysis show that penetration down into the structure is allowable, different failure criteria could be assigned to the 13 regions.

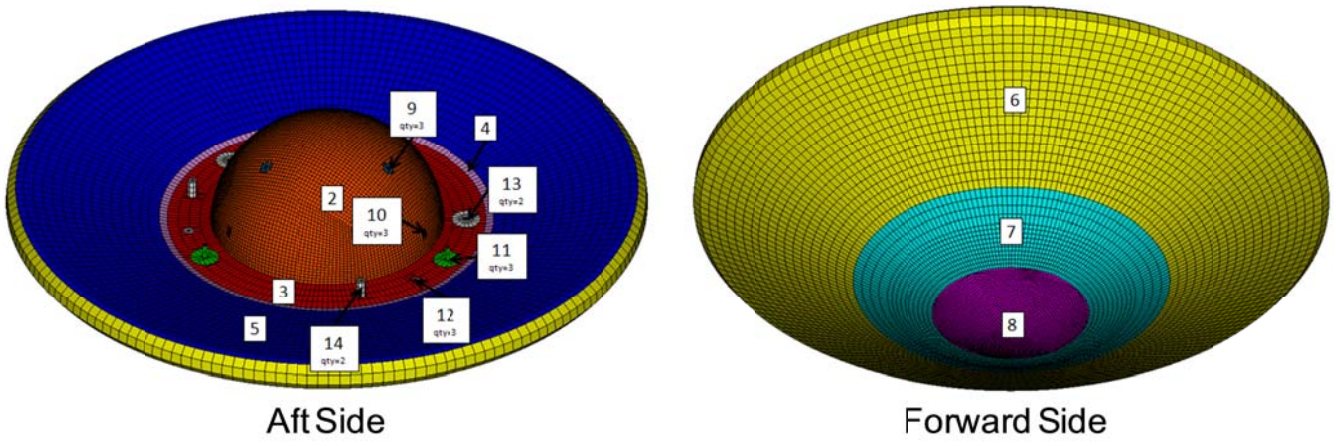

Figure 4-2. MSR EEV Analysis – Finite Element Model.

However, for this analysis each of the 13 regions was given one of two failure criteria: penetration through the thickness of the forward TPS or penetration through the thickness of the aft TPS structure. Furthermore, should it be necessary to use failure criteria similar to the Orion TPS, then the failure criteria will vary from the windward to the leeward sides, and it will be necessary to add more regions to the finite element model.

The I-DEAS finite element model variable that is mapped into the failure criterion used by BUMPER-II is called a property ID (PID). Thus, each of these 13 risk regions called a PID in this report. Some of the geometric characteristics of the 13 PIDs are listed in Table 4-1. The first column lists the PID number used in the I-DEAS universal file. The second column lists the label assign to the PID by the finite element modeler. The third column lists whether the PID was assigned an aft TPS failure criterion or a forward TPS failure criterion. The fourth column lists the color of the PID in Figure 4-2. The fifth, sixth and seventh columns list the starting element ID for the PID, the ending element ID, and the total number of elements in the PID, respectively. The eighth column lists the surface area of the PID in square meters.

Table 4-1. MSR EEV Analysis - Risk Region, PID, EID and Area Map.

MSR EEV FEM - Risk Region, PID, EID, and Area Map							
PID #	Risk Region	TPS Side	Color	Element ID Range			Surface Area (m^2)
				Start ID	End ID	Total	
1	Shadowing	---	white	---	---	0	0.000
2	LID TPS (No-MLI)	Aft	orange	1001	7445	6445	0.155
3	Aft TPS (Body Foam, No-MLI)	Aft	red	8001	8801	801	0.068
4	Aft TPS (Gap, No-MLI)	Aft	pink	9001	9184	184	0.016
5	Aft TPS (MLI, Gap)	Aft	blue	10001	12760	2760	0.438
6	Fwd TPS (MLI, Gap)	Forward	yellow	13001	16864	3864	0.646
7	Fwd TPS (MLI, Body Foam)	Forward	cyan	17001	19576	2576	0.134
8	Fwd TPS (Double MLI, Gap)	Forward	magenta	20001	22484	2484	0.040
9	LID Push Pad	Aft	lt blue	23001	23048	48	0.001
10	LID Pin	Aft	yellow	24001	24048	48	0.000
11	Body Mount Bolt	Aft	green	25001	25144	144	0.005
12	Unknown 1	Aft	white	26001	26024	24	0.000
13	Unknown 2	Aft	white	27001	27064	64	0.002
14	Unknown 3	Aft	white	28001	28064	64	0.002
					Total:	**19506**	**1.507**

The EEV is transported to Mars and then back to the vicinity of Earth by a carrier vehicle. This is illustrated in the graphic shown in Figure 4-3. The 2018 launch on the left hand side of the plot lands a rover on Mars to collect samples and rendezvous with the Mars ascent vehicle. The 2022 launch sends the MSR orbiter to Mars with the EEV. The third and final launch in 2024 sends the MSR lander with ascent vehicle to Mars. The lander inserts a specimen (the orbital sample or OS) in the ascent vehicle and the ascent vehicle rendezvous with the orbiter. The orbiter then leaves Mars and releases the EEV in the vicinity of Earth for Earth entry.

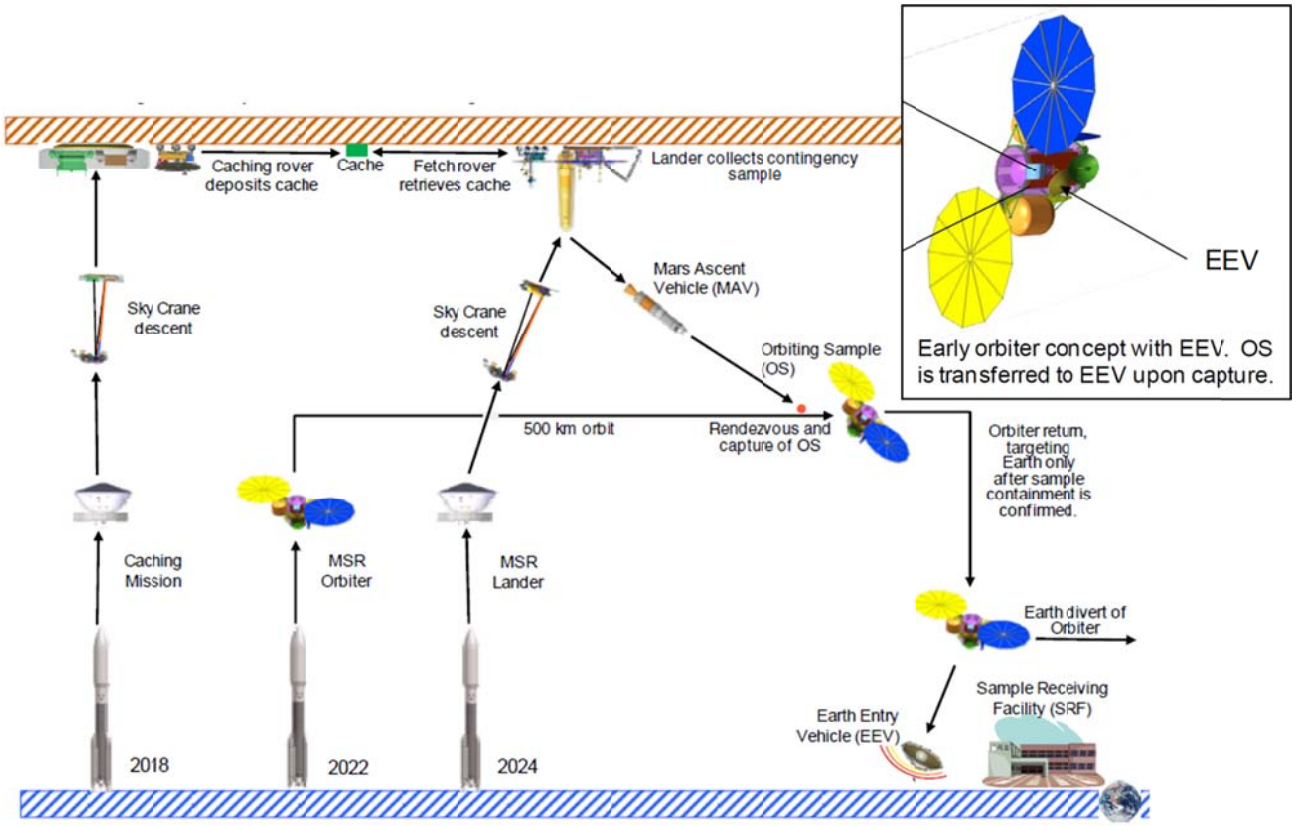

Figure 4-3. MSR EEV Analysis - Mission Configuration (Mattingly and May, 2011).

This orbiter is much larger than the EEV as shown in the upper right inset of Figure 4-3 with the dark yellow EEV mated to the side of the orbiter. The large orbiter shadows the EEV from the meteoroid environment for the majority of the mission, reducing the risk of meteoroid impact on the aft TPS. A notional model of the orbiter was constructed using a cylinder as shown in Figure 4-4.

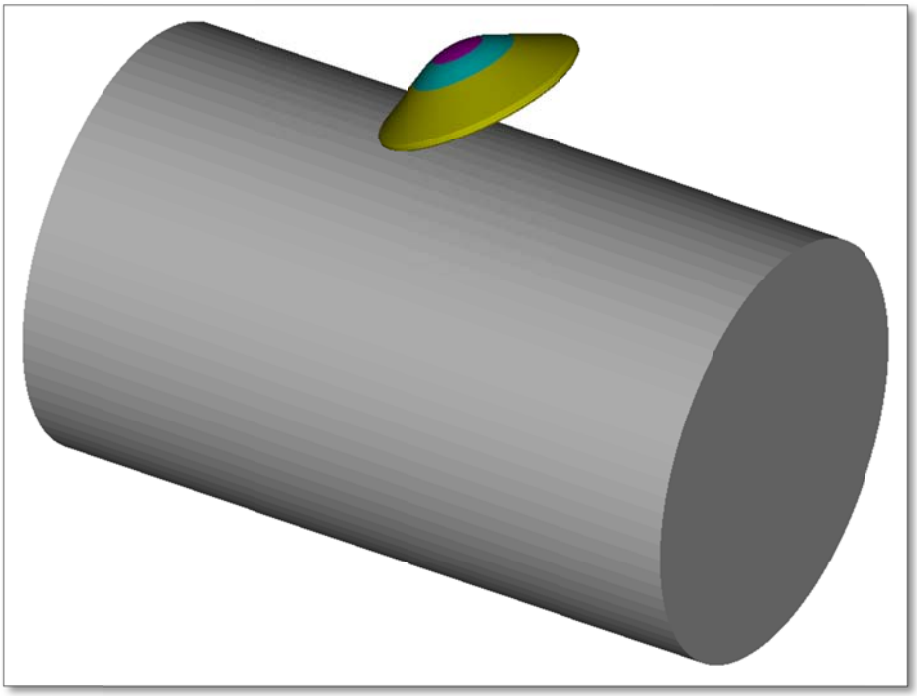

Figure 4-4. MSR EEV Analysis – EEV FEM with Transit Vehicle.

Additionally, a FEM with the EEV completely enclosed in an MMOD "garage" (for all mission phases up to Earth reentry) was used for a concept study and is shown in Figure 4-5.

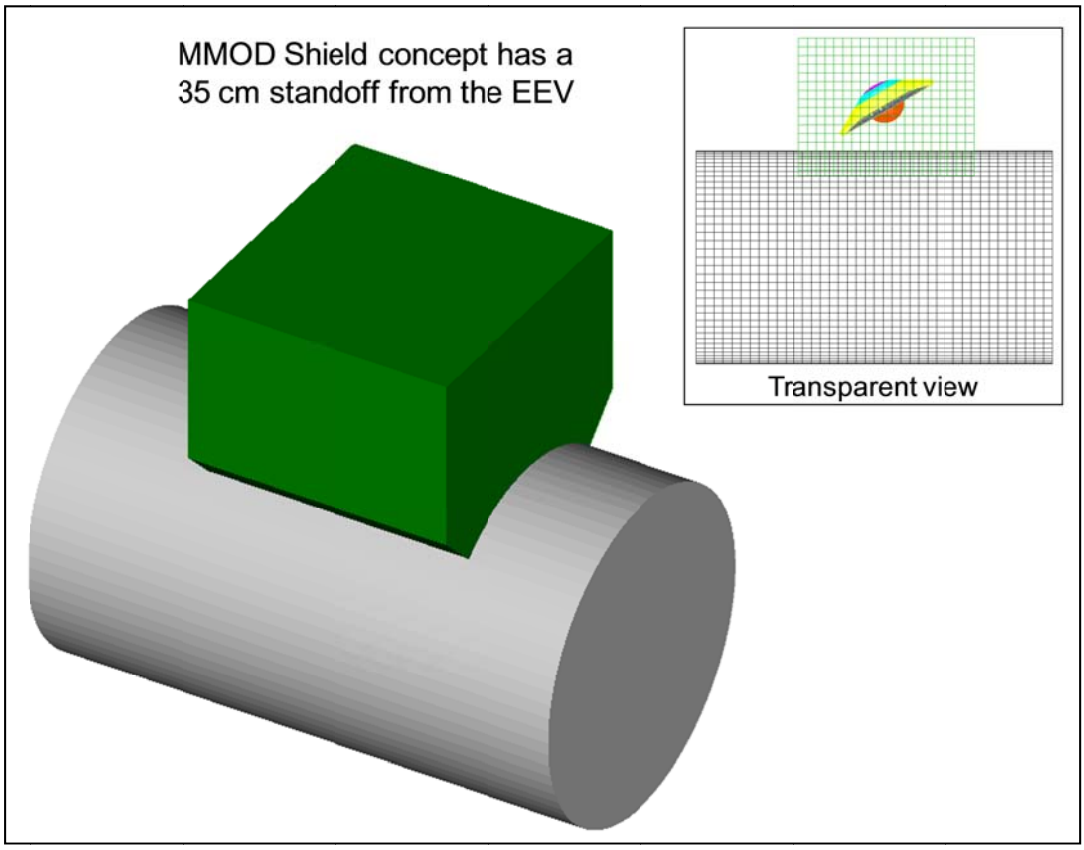

Figure 4-5. MSR EEV Analysis - MMOD Shield Concept FEM.

4.3 Assessment Inputs

MSR EEV analysis parameters are summarized in Table 4-2. Version "CEV 1.73" of the BUMPER-II code was used for the assessment. The current orbital debris engineering environment, ORDEM2000 was used with a constant projectile density of 2.8 grams per cubic centimeter. The MEM environment was used for meteoroid risk calculations. IP MEM v2.1 was used for the transit phases and MarsMEM was used for the orbital phase. Additional information is available in section 4.4.3.

Table 4-2. MSR EEV Analysis Parameters.

MSR EEV Analysis Parameters	
Parameter	**Value**
Analysis Code	BUMPER-II CEV v1.73
Debris Environment	ORDEM2000
Debris Density	Constant 2.8 g/cm^3
Number of Debris Threat Cases	90
Meteoroid Environments	IP MEM v2.1 & MarsMEM
Number of Meteoroid Threat Cases	1652

The MSR EEV mission consists of 15 phases (Table 4-3) from launch of the MSR EEV (with transit vehicle) to reentry of the EEV only. The total exposure duration of the MSR EEV to the MMOD environments is approximately 4.83 years. For this analysis, meteoroid impacts during the launch/LEO and EEV reentry phases were ignored. Additionally, only orbital debris impacts during EEV reentry were considered.

Table 4-3. MSR EEV Analysis - Mission Phases.

MSR EEV Mission Phases			
Mission Phase		Exposure Time (yr)	Comments
1	Launch-LEO	0.00023	2 hrs, ignored meteoroids and OD
2	Earth to Mars transit	0.70833	8.5 months
3-11	Mars Arrival (aerobraking)	0.41096	150 days (9 non-circular orbits considered)
12	Mars Orbit	3.00000	Circular orbit (alt = 572km)
13	Mars departure orbit	0.00548	48 hrs
14	Mars to Earth transit	0.70833	8.5 months
15	EEV Entry	0.00023	2 hrs, assessed OD, ignored meteoroids
	Total	**4.83356**	

Due to the preliminary status of the MSR EEV mission design, the attitude of the MSR transit vehicle has not been determined. Therefore the approach taken for the MSR EEV analysis was to use 24 attitudes (90° rotations about the axes of the spacecraft coordinate system) for the mission phases while the EEV is attached to the transit vehicle. These 24 attitude cases were used only with the meteoroid environment (orbital debris only considered during EEV Earth reentry) and are summarized in Table 4-4. The rotations are expressed in a "Bumper Roll, Pitch, Yaw" or "RPY" space fixed sequence, where "Roll" is a rotation about the "X" axis of the reference frame, "Pitch" is a rotation about the "Y" axis and "Yaw" is a rotation about the "Z". The XYZ reference frame for the attitude cases is illustrated in Figure 4-6.

Table 4-4. MSR EEV Analysis – Meteoroid Attitude Cases.

MSR EEV Attitude Cases			
	Bumper RPY		
Case #	X	Y	Z
1	0	90	0
2	90	90	0
3	180	90	0
4	270	90	0
5	0	270	0
6	90	270	0
7	180	270	0
8	270	270	0
9	0	0	0
10	0	0	270
11	0	0	180
12	0	0	90
13	180	0	180
14	180	0	90
15	180	0	0
16	180	0	270
17	90	0	0
18	90	0	270
19	90	0	180
20	90	0	90
21	270	0	180
22	270	0	90
23	270	0	0
24	270	0	270

Additionally, the 24 attitude cases are depicted graphically in Figure 4-6. Further information regarding the coordinate system used for the meteoroid environment can be found in Appendix E - MEM Coordinate System.

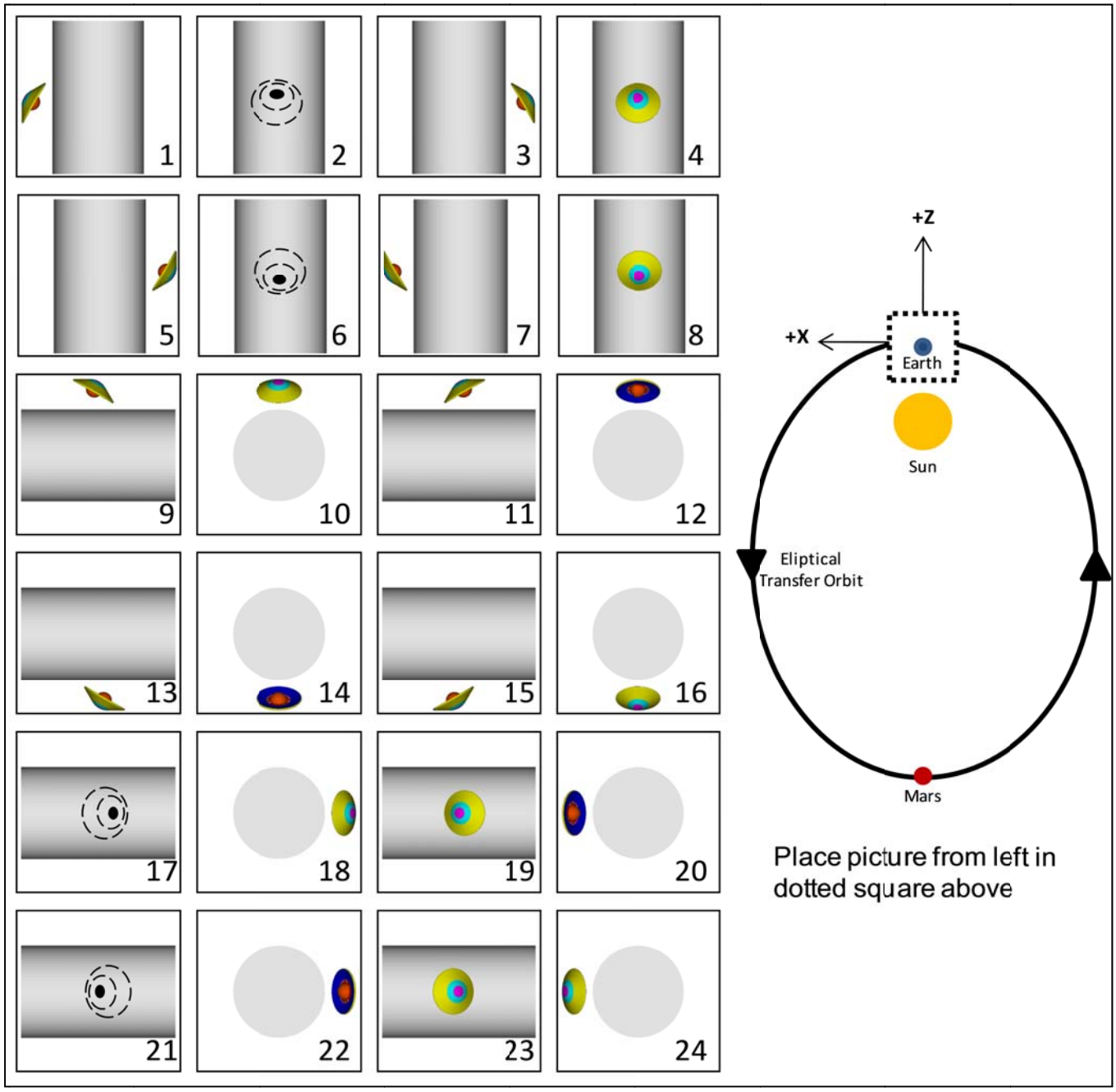

Figure 4-6. MSR EEV Analysis – 24 Meteoroid Attitude Cases.

For the EEV Earth reentry phase (orbital debris only), a single attitude (Figure 4-7) was considered with the EEV pitched down 20° with respect to the local horizontal. The selection of the Earth reentry trajectory and attitude is discussed in Section 4.4.1.5.

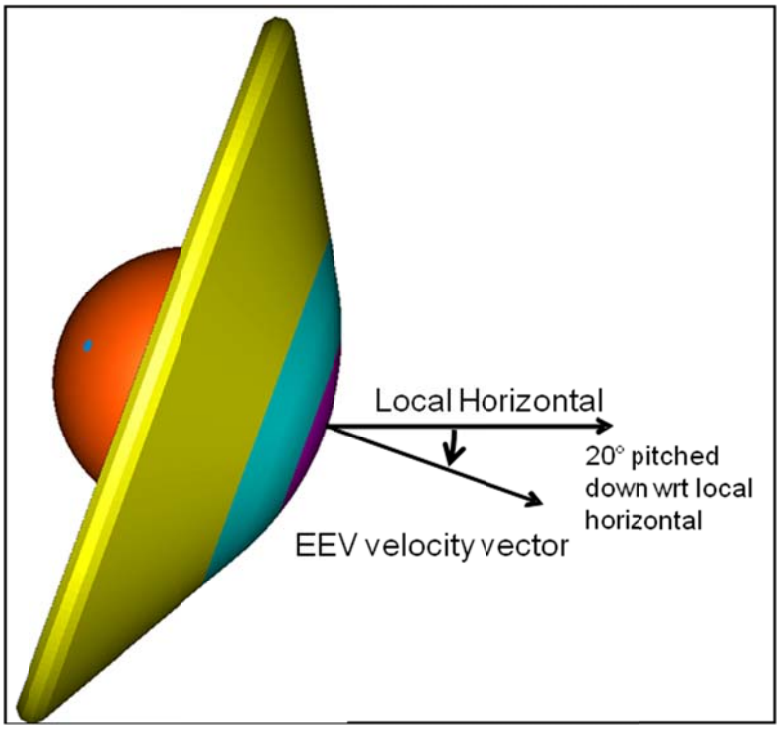

Figure 4-7. MSR EEV Analysis - EEV Earth Reentry Attitude.

4.4 Environment Models

4.4.1 Trajectory

The spacecraft trajectory through the orbital debris and the meteoroid environments is one of the factors that determine the penetrating fluence of particles. The MSFC Meteoroid Environment Office used recent Mars spacecraft trajectories to bound the range of possible meteoroid fluence. Bill Cooke's discussion of the reasoning used to select trajectories for the meteoroid impact analyses is reproduced below from a June 2011 email.

The time of flight in low Earth orbit for both outbound and inbound trips is approximately 1.75 hours, which is not a significant amount of time exposed to the meteoroid environment. It is not necessary to model these phases of the mission for the number of impacts by meteoroids analysis. (However, it is necessary to analyze these phases to determine the orbital debris fluence. While the orbital debris fluence is small, the mean number of impacts requirement is orders of magnitude smaller than the requirement for other spacecraft analyzed by JSC/KX engineers to date. The discussion of the earth entry trajectory used in the number of impacts by orbital debris particles appears in Section 4.4.1.5.)

The exact trajectory for the Earth-Mars-Earth interplanetary cruise is unknown. Several NASA Mars missions were investigated and their interplanetary flight paths were used to generate meteoroid environment files and bound the possible variations in flux due to unknown flight path. The following mission trajectories were readily available from the JPL Horizons website in the necessary format: Mars Exploration Rover – Spirit, Mars Exploration Rover – Opportunity, Mars Reconnaissance Orbiter (MRO), and Mars Odyssey. Mars Pathfinder orbital elements for half of the interplanetary cruise were located on the mission webpage and used for comparison. Also, a simple Earth-Mars-Earth Hohman trajectory was generated for comparison. The Spirit and Opportunity missions represent "type 1" interplanetary transfers, the fastest possible. The cruise phases lasted 5 months. MRO and Odyssey had longer cruise phases of 7 months and a Hohman minimum-energy transfer represents the longest case with a cruise time of 8.5 months.

Since the meteoroid environment directionality is fixed with respect to the Sun, the spacecraft can be exposed to different sources of meteoroids depending on its flight path and attitude. It is assumed this spacecraft is not rotating and the ram surface (X) is defined by the spacecraft's velocity vector, port surface (Y) is defined by the angular momentum vector and zenith surface or space facing surface (Z) is the cross product of the velocity vector and angular momentum vectors.

Upon insertion into Mars orbit, the spacecraft spends 150 days aerobraking into a circular orbit. This aerobraking phase was simulated by generating orbits at various apoapse altitudes but with the same inclination, node and periapse altitude. It is not

known how long the spacecraft will spend at each altitude so an average environment was constructed over one orbit at each altitude during this aerobraking phase.

The spacecraft trajectories from JPL Horizons used for the Earth to Mars and the Mars to Earth transit phases and the Keplerian elements used for the elliptical orbit phases are listed in Table 4-5. These choices are described in greater detail in what follows. The first column of Table 4-5 lists the mission phase ID number, the second the mission phase label, the third the trajectory type, the fourth the Mars apoapse for mission phases 3 to 13 and the Earth apoapse for mission phase 15, the fifth column the Mars periapse for mission phases 3 to 13 and the Earth periapse for mission phase 15, the sixth column lists the right ascension of ascending node, the seventh column lists the argument of perigee, the eighth column the orbital period and the ninth column the inclination of the orbit.

Table 4-5. Spacecraft Trajectories and Keplerian Elements for the 15 Mission Phases.

	Mission phase	Trajectory	Apoapse (km)	Periapse (km)	Node	ω (deg)	Period (hrs)	Inclination (deg)
1	Launch-LEO	Not analyzed						
2	Earth to Mars transit	Spirit, MRO, Hohman						
3	Mars Arrival (aerobraking)	1 orbit	60,000	3,897	152		48	45
4	Mars Arrival (aerobraking)	1 orbit	49,811	3,897	152		37	45
5	Mars Arrival (aerobraking)	1 orbit	39,142	3,897	152		27	45
6	Mars Arrival (aerobraking)	1 orbit	29,526	3,897	152		18	45
7	Mars Arrival (aerobraking)	1 orbit	19,252	3,897	152		11	45
8	Mars Arrival (aerobraking)	1 orbit	14,234	3,897	152		7	45
9	Mars Arrival (aerobraking)	1 orbit	9,858	3,897	152		5	45
10	Mars Arrival (aerobraking)	1 orbit	4,087	3,897	152		2	45
11	Mars Arrival (aerobraking)	1 orbit	4,084	3,957	152		2	45
12	Mars Orbit	1 orbit	3,965	3,956	TBD		2	45
13	Mars departure orbit	1 orbit	60,000	3,697	152		48	45
14	Mars to Earth transit	Hohman						
15	EEV Entry	Genesis (EI-2 hrs to EI)	1,382,034	6,378	…	90	1,599	32.2

4.4.1.1 Launch Phase

An MSR reference trajectory for launch is unavailable for use in generating an average environment file. However, by definition, a launch trajectory is a power track, and hence hyperbolic in Earth centered inertial (ECI) coordinates. This was confirmed by using JPL Horizons to calculate the MRO launch trajectory. The launch phase covers the first 2 hours of mission elapsed time.

4.4.1.2 From Earth to Mars Cruise Phase

An MSR reference trajectory to Mars is unavailable for use in generating an average environment file; however several recent NASA missions have their interplanetary cruise trajectories available on the JPL Horizons website. In order to describe and bound the meteoroid environment for this phase of the mission, three trajectories were used to develop the meteoroid flux-direction files. The Mars Exploration Rover – Spirit trajectory was chosen because it followed a "type 1" interplanetary transfer, the fastest possible, arriving at Mars in 5 months. The MRO spacecraft trajectory was chosen because it had a 7 month interplanetary cruise approaching Mars from the south and was typical of an average transit time. Finally, a minimum-energy Hohman transfer trajectory was used where the cruise phase lasted about 8.5 months.

4.4.1.3 Aerobraking, Mars Orbit and Mars Departure Phases

While some information was available for the initial orbit, other information had to be assumed in order to approximate a set of environment files for several different orbit orientations. There are 11 meteoroid environment files that describe the meteoroid environment during the aerobraking phase, Mars orbit and Mars departure orbit phases. The aerobraking phase occurs over 150 days, 10 orbits were constructed to simulate the falling apoapse. The last file represents the final orbit where the vehicle is presumed to spend the most time before raising the apoapse for the Mars departure orbit. Each file represents the "average" and 1 sigma environment over 1 orbit at that altitude sampled in 60 second time steps.

The orbit parameters at Mars were described by the following: an initial orbit with period = 48 hours, periapse altitude = 500 km, inclination = 45 degrees, Node-IAU = 15.6 degrees, argument of periapse = -0.2 degrees, and Mean anomaly = 0 degrees at 12:00 ET on 7/10/2023. IAU is a vector defined in a Mars centered coordinate frame. The IAU- vector is defined to be

along the intersection of the Mars Mean Equator of Date plane and the Earth Mean Equator of Epoch J2000 plane, and is positive in the direction of the ascending node of the Mars mean equator of date on the Earth mean equator of epoch J2000. This vector can be found using a relationship between the vernal equinox vector and the angle between the IAU vector and equinox. This angle is about 136 degrees. Substituting the IAU angle in the above equation we can solve for the Node location of the orbit plane which is around 152 degrees. This IAU vector and Mars coordinate frames are described in an interoffice memorandum 343B-2006-004 dated August 15, 2006 from NASA JPL. An STK scenario was developed using Astrogrator's "Targeter" to simulate the initial Mars orbit, aerobraking phase, and final orbit mission for MSREEV. State vectors were found in a Mars centered inertial J2000 reference system for input into MarsMEM, for each orbit segment described above. Once the aerobraking phase ends the spacecraft resides in a more circular orbit with altitude of 572 km and inclination of 45 degrees, the node is "TBD". The orbiter then rendezvous with the Mars surface sample at an unknown altitude between the ranges of 522-572 km for both periapse and apoapse distances. Sometime over the next 3 years between December 2023 and July 2026, the orbit period is raised to somewhere between 2 hours and 48 hours and then over a period of a few days in July 2026, the periapse is lowered to 300 km and apoapse is raised (if not already there) to a period of 48 hours just before the trans-Earth insertion maneuver.

4.4.1.4 From Mars to Earth Cruise Phases

For the interplanetary return phase of the mission, there were no specific trajectories described, and no recent NASA Mars missions to model this. A Hohman transfer orbit was again used to describe the state vectors over the return trip. States were sampled in 1 day time increments over 8.5 months.

4.4.1.5 EEV Entry

The Genesis trajectory was selected as an example of an Earth return vehicle reentry trajectory. The JPH Horizons web site was used to generate the Keplerian elements in Earth centered coordinates of the last two hours of the Genesis trajectory. The header for the Horizons output file documents the input parameters used to generated the trajectory and is included as Section 9 of this report. The Keplerian elements from Horizons are plotted in Figure 4-8. The elements are constant until the last 8 minutes before entering the Earth's atmosphere (Earth interface), so the constant values were used for the whole trajectory. These are listed in Table 4-5. (Two hours corresponds to 7,200 seconds, during which time the Genesis sample return capsule traveled from 34,000 km altitude to Earth interface. Geosynchronous orbit is about 36,000 km altitude, so for the last two hours of the trajectory the Genesis Earth return capsule was within the Earth orbital debris belt.)

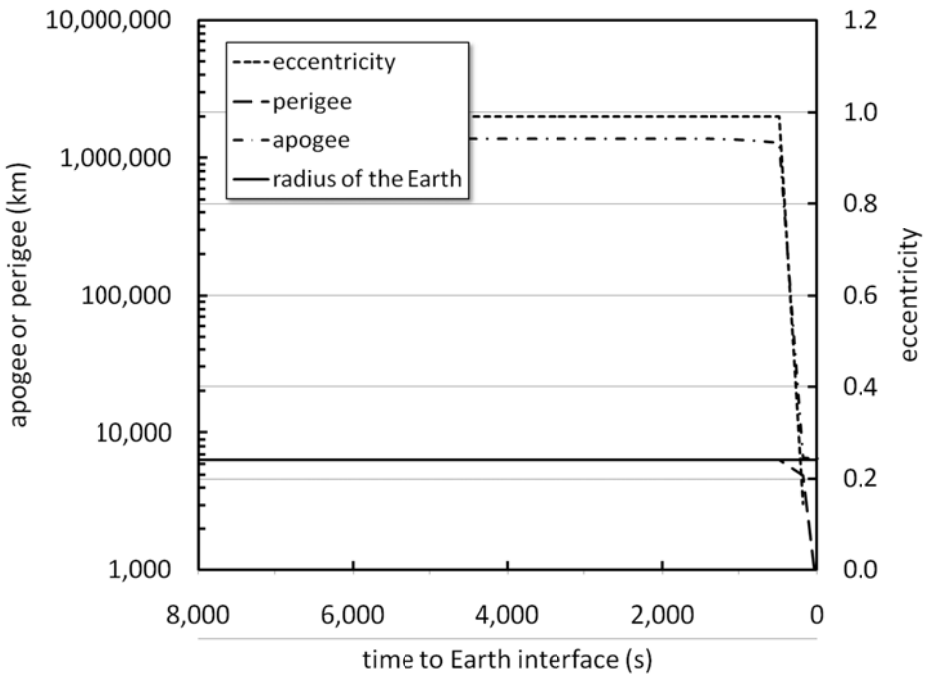

Figure 4-8. Keplerian elements from JPL Horizons for the last 2 hours of the Genesis orbit before Earth Interface.

The spacecraft attitude during reentry was estimated by assuming the apex of the forward TPS cone was pointed in the spacecraft velocity direction. The scalar product of the spacecraft position vector and the spacecraft velocity vector was then computed to obtain the cosine of the angle between the position vector and the velocity vector. The spacecraft position vector

is normal to the local horizontal, hence the angle between the spacecraft position vector and the spacecraft velocity is the complement of the angle the spacecraft velocity makes to the local horizontal. This angle is cross plotted with the spatial density of 1 mm orbital debris particles during the year 2005 for altitudes above the equator. The maximum spatial density occurs for angles with respect to the local horizontal around 20 degrees, which was used for the attitude over the whole of the Earth entry phase.

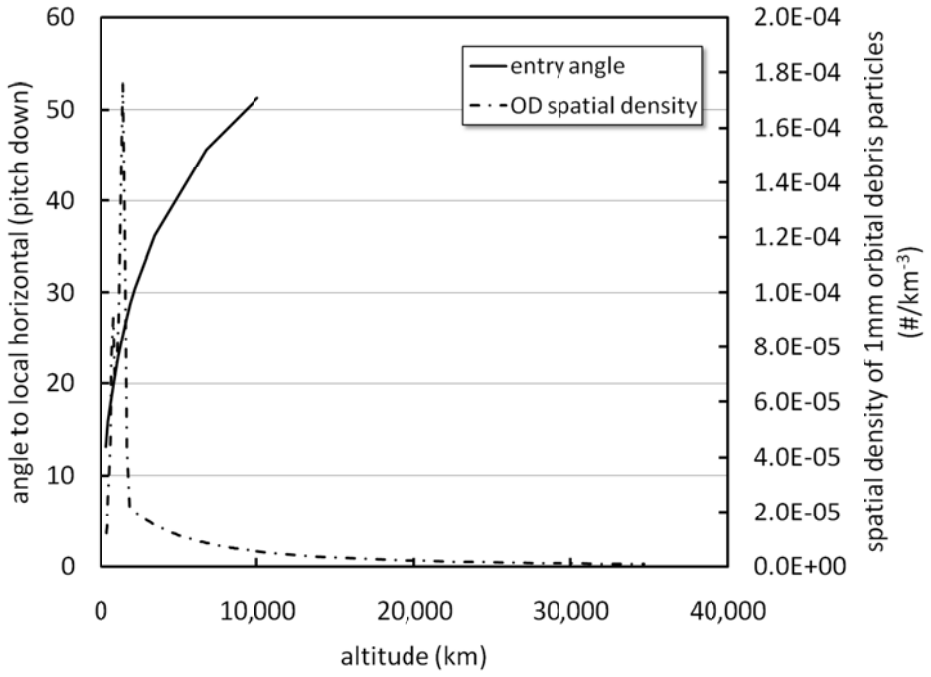

Figure 4-9. EEV attitude as a function of altitude cross plotted with the spatial density of 1 mm diameter orbital debris particles as a function of altitude.

4.4.2 Orbital Debris Environment

The ORDEM2000 orbital debris environment model (Liou, et al. 2002) was used for the Earth entry phase of the analysis. ORDEM2000 is the latest released version from the JSC Orbital Debris Program Office (ODPO) and is valid up to 2000 km altitude. Bjorkman (with Matney's concurrence) extended the ORDEM2000 environment to larger altitudes by extrapolating the orbital debris spatial density at 2,000 km using an inverse square dependence on radial distance from the center of the Earth. This extrapolation is apparent as the smooth function between 2,000 and 36,000 km in Figure 4-9. The extrapolation between 2,000 and 36,000 km altitude is thought conservative, perhaps by a wide margin. The degree of conservatism that the extrapolation has added to the results is unknown. The soon to released ORDEM 3.0 environment will calculate flux on spacecraft from LEO to GSO, and could provide a check on the analyses performed for the EEV.

The orbital debris flux varies with the solar activity during the 11 year solar cycle. Years of high solar activity heat the atmosphere and increase the rate of orbital debris orbital decay. These years have a small flux. Years of low solar activity have less solar heating of the atmosphere, less orbital decay, and relatively larger fluxes. The oscillation of the orbital debris flux with the 11 year solar cycle is superimposed on a more uniform rate of flux increase resulting from the accumulation of material in Earth orbit from the historically more-or-less constant launch rate. Since the MSR Earth return vehicle is assumed to reenter Earth's atmosphere in the year 2026, these two factors involve a 25 years extrapolation from the creation date of the ORDEM2000 environment model. The effect of changes in the period of the solar cycle and the historical launch rate on the ORDEM2000 prediction of the orbital debris flux in 2026 have not been considered.

A third, and more restrictive, ORDEM2000 use limitation is that it only calculates the orbital debris flux on spacecraft in closed elliptical orbits around the Earth. The MRO launch trajectory was computed in ECI coordinates with JPL-Horizons, but was found to be hyperbolic, hence not suitable for use with ORDEM2000. The Genesis sample return capsule entry trajectory was calculated with JPL-Horizons and was found to be elliptic and could be used with ORDEM2000. Thus this EEV analysis only considers orbital debris impacts during the Earth entry phase and not during launch. This may not be a significant oversight if meteoroid shields are added to the EEV bio-shield. If they are, then the risk of EEV TPS failure due to orbital debris impact may be significantly smaller than the risk during entry, when there is no shield. If it isn't possible to add

meteoroid shields to the bio-shield, then the TPS risk of failure during launch, may be as large as during entry, and shouldn't be overlooked.

Bjorkman recently modified ORDEM2000 to output the flux for segments of an elliptical orbit. This modification was used to calculate the flux during the last 2 hours of the Genesis entry using the Keplerian elements listed in Table 4-5. However, ORDEM2000 is coded to divide an elliptical orbit into no more than 9,999 segments, so the last two hours of the extremely elliptical Genesis entry orbit covered only 13 segments. The cross sectional area flux for those 13 segments were written out and cross plotted with the spatial density of 1 mm size orbital debris particles during the year 2005 above the equator.

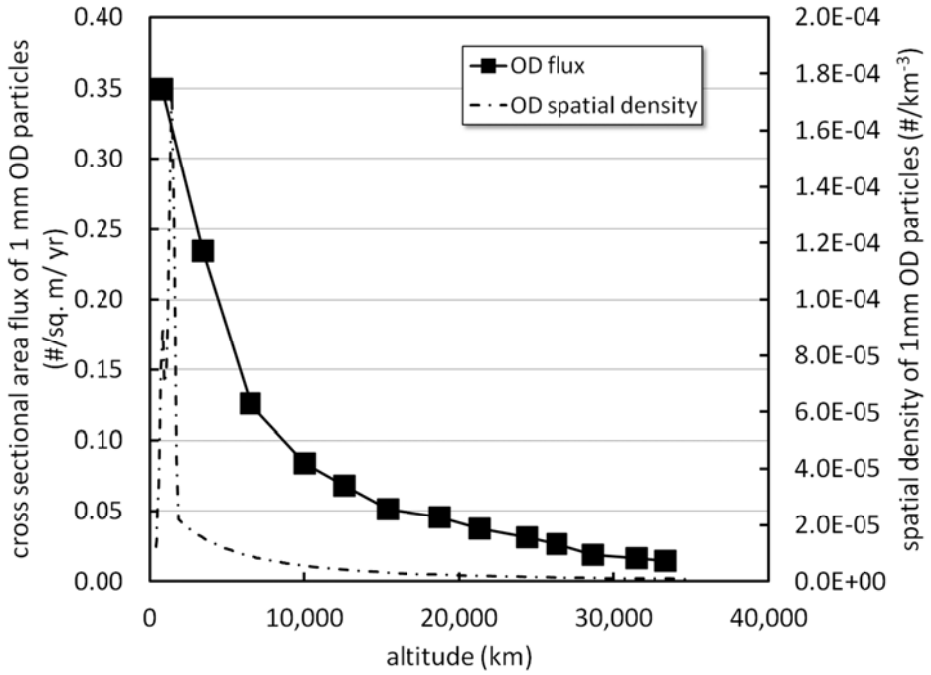

Figure 4-10 . Flux of 1 mm OD particles on the EEV as a function of altitude cross plotted with the spatial density of 1 mm diameter orbital debris particles as a function of altitude.

The plot illustrates two issues. First, 12 of the 13 points lie at altitudes above 2,000 km, and these 12 points add up to 68% of the orbital debris fluence on the EEV during entry. The flux from altitudes above 2,000 km was computed from an extrapolation of the spatial density. The extrapolation function was selected because it was thought to give a conservative answer. The degree of conservatism is unknown and won't be quantifiable until the ORDEM2010 environment is released. The second issue is the spatial density rapidly varies with altitude below 2,000 km and the flux for altitudes below 2,000 km has been approximated by only one flux; the flux at 820 km altitude.

Regardless of the issues, estimates of the impacting and penetrating flux were made with the existing ORDEM2000 orbital debris environment model. Should the ORDEM2000 results raise issues with the EEV design, then it may be prudent to modify the ORDEM 3.0 orbital debris environment model for EEV and recalculate the probability of TPS failure before modifying the EEV design.

4.4.3 Meteoroid environment

The MSFC Meteoroid Environment Office (MEO) provided a description and 13 models of the meteoroid environments for the applicable mission phases (Cooke, 2011). (See (McNamara et al, 2004) for a description of the MEM computer program used to generate the environments.) The mission phase number, mission phase label, meteoroid environment file name, and cumulative cross sectional area flux of 1 microgram or larger meteoroids are listed in columns 1 to 4 of Table 4-6, respectively.

Table 4-6. Environment Files Used for the Fifteen Mission Phases.

ID	Mission phase	MEM.DAT or ORDEM2K.DAT file name	Cross sectional area flux of 1 microgram meteoroids (#/sq m/yr)
1	Launch-LEO	N/A	
2	Earth to Mars transit	AvgOutIPMEMIgloo.out	4.138±0.570

ID	Mission phase	MEM.DAT or ORDEM2K.DAT file name	Cross sectional area flux of 1 microgram meteoroids (#/sq m/yr)
3	Mars Arrival (aerobraking)	abo1_AvgMEMIglooDist.out	1.656±0.278
4	Mars Arrival (aerobraking)	abo2_AvgMEMIglooDist.out	1.658 0.278
5	Mars Arrival (aerobraking)	abo3_AvgMEMIglooDist.out	1.657±0.277
6	Mars Arrival (aerobraking)	abo4_AvgMEMIglooDist.out	1.656±0.276
7	Mars Arrival (aerobraking)	abo5_AvgMEMIglooDist.out	1.649±0.274
8	Mars Arrival (aerobraking)	abo6_AvgMEMIglooDist.out	1.646 0.274
9	Mars Arrival (aerobraking)	abo7_AvgMEMIglooDist.out	1.630±0.271
10	Mars Arrival (aerobraking)	abo8_AvgMEMIglooDist.out	1.451±0.245
11	Mars Arrival (aerobraking)	abo9_AvgMEMIglooDist.out	1.458±0.247
12	Mars Orbit	abo10_AvgMEMIglooDist.out	1.458±0.246
13	Mars departure orbit	FinalOrbitAvgMEMIglooDist.out	1.662±0.300
14	Mars to Earth transit	AvgInIPMEMIgloo.out	3.898±0.603
15	EEV Entry	ORDEM2K-rentry.dat	

The cumulative cross sectional area flux values listed in column 4 as a function of mission phase reflect the decrease in spatial density of meteoroids with heliocentric radial distance. The cumulative cross-sectional flux of meteoroids in Earth space at 1 AU is approximately 5.95 $m^{-2}yr^{-1}$ for particles down to 1 microgram. At Mars this flux drops to about 2.34 $m^{-2}yr^{-1}$ with an average speed of 18.2 km/s.

The cross sectional area flux listed in Table 4-6 is listed with the estimate of standard deviation made by engineers at the Meteoroid Environment office. The method used to estimate the standard deviation is discussed in Section 4.4.3.4.

The environment files are required because the background or “sporadic” meteoroid environment is not isotropic. Each file is a table of flux values for a distribution of approach angles. The distribution of approach angles comes from the 6 sources of meteoroids. Comets contribute the majority of the meteoric material in the inner solar system and asteroids contribute a much smaller portion. Within 1.5 AU, the sporadic sources appear fixed in their direction about the Sun. In the heliocentric ecliptic frame, the most active sources are the helion and anti-helion source which appear to come from a direction near the Sun and opposite the Sun, respectively. The next most active sources are the North and South toroidal which radiate from high above the ecliptic plane, about ±60 degrees centered on the direction of motion about the Sun. The last two sources are the weakest in contribution but are the fastest particles, called the North and South Apex and are located ±20 degrees also centered on the direction of motion about the Sun. Figure 4-11 depicts the radiant distribution at Earth of sporadic meteoroids for the larger threat size particles with masses greater than 100 micrograms. This figure is what the Earth sees on its trajectory around the Sun. Even though Mars is on a slightly more eccentric path the sources still appear to radiate from the same direction relative to the Sun and Mars’ motion.

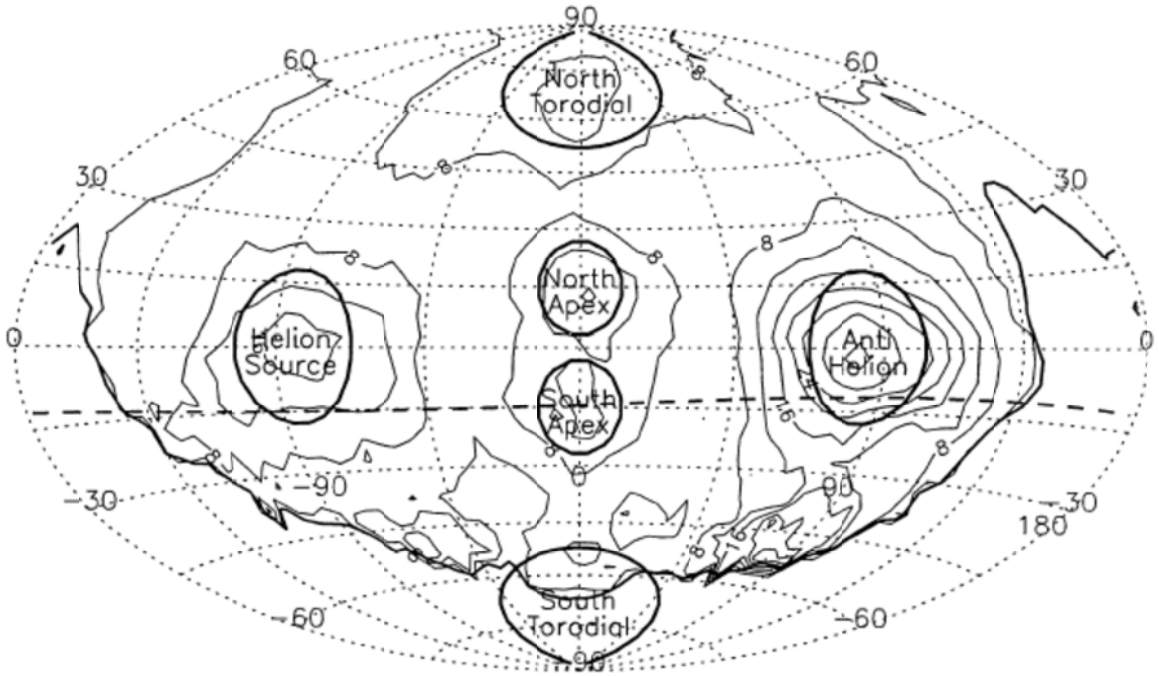

Figure 4-11. Radiant distribution of sporadic meteoroids as seen by Earth in heliocentric ecliptic plane. Image from (Taylor and McBride, 1997).

All environment files describe the cumulative cross-sectional flux of meteoroids down to a limiting mass of 10^{-6} grams. Particle density is assumed to be 1.0 g/cm^{-3}, the average density of cometary material, which comprises the majority of meteoric material in the inner solar system.

The Meteoroid Environment Office specified the following relation for scaling the flux of 1 microgram meteoroids to larger meteoroid masses.

$$F = F_0 \left(\frac{m}{1\times10^{-6}\,\mathrm{g}}\right)^{-1.34} \qquad (1)$$

The variable F is the cumulative cross sectional area flux of meteoroids with mass m or larger. The parameter F_0 is the cumulative cross sectional area flux of 1 microgram or larger meteoroids read from the environment files. Both F and F_0 have units of number of meteoroids per square meter per year. The mass m has units of grams.

The following subsections describe the method used to calculate the MEM meteoroid environment files for the mission phases listed in Table 4-6.

4.4.3.1 From Earth to Mars Cruise Phase:

The Interplanetary Meteoroid Engineering Model (IPMEM v 2.1) was used to calculate an average meteoroid environment file over the interplanetary cruise phase for Spirit, Mars Reconnaissance Orbiter (MRO) and a simple Hohman transfer. These three missions represent different trajectories to Mars with varying transfer times. State vectors were selected using the same time step between each of their Earth departures and Mars arrivals. These three trajectories were analyzed separately to generate an average meteoroid environment over the cruise portion of each mission, then the files were averaged to produce the environment file.

Figure 4-12 is a plot of the cumulative cross sectional area flux of meteoroid one microgram or larger factored into 5 km/s closing speed bins for the outbound interplanetary cruise portion of the mission.

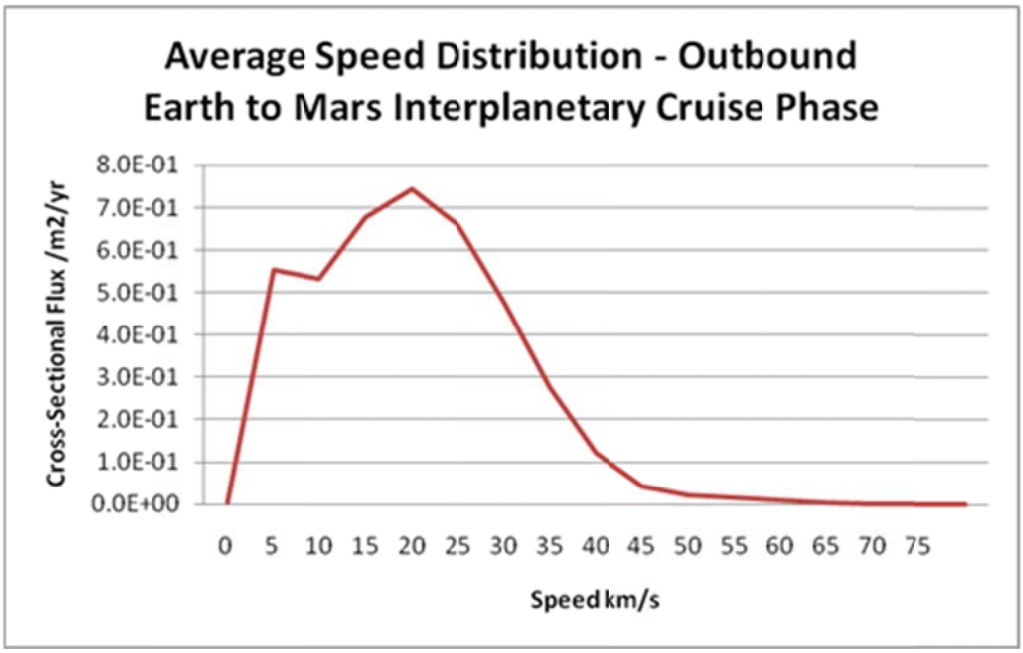

Figure 4-12. Cumulative flux of sporadic meteoroids distributed by 5 km/s speed bins for masses of one microgram or larger over the outbound interplanetary cruise portion of the mission; generated using average environments from the interplanetary cruises of Spirit, MRO and a simple Hohman transfer.

4.4.3.2 Mars Arrival and Orbit

There are 11 meteoroid environment files that describe the meteoroid environment during the aerobraking phase and final rendezvous phase before trans-Earth insertion. These files were generated using a newly developed meteoroid environment model, MarsMEM. This version of MEM includes Mars as the central body so that the correct planetary gravitational focusing and shielding will be used. The names of the environment files generated with MarsMEM are listed by mission phase in Table 4-6. The aerobraking phase of the trajectory was assumed to occur over 150 days. Ten orbits were constructed to simulate the falling apoapse. The Phase 12 file represents the final orbit where the vehicle is presumed to spend the most time before trans-Earth insertion. Each file is taken as representative of an "average" environment for that phase.

Figure 4-13 is a plot of the cumulative cross sectional area flux of meteoroids 1 microgram or larger factored into 5 km/s closing speed bins for the Mars orbit phase of the mission.

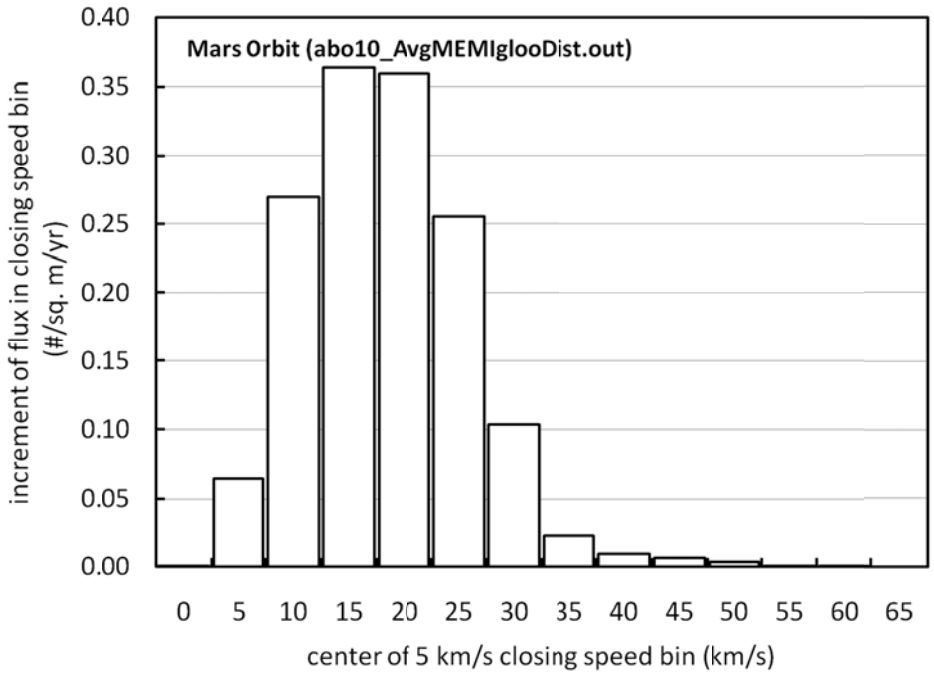

Figure 4-13. Cumulative flux of sporadic meteoroids distributed by 5 km/s speed bin for masses of one microgram or larger onto a spacecraft in Mars orbit.

4.4.3.3 From Mars to Earth Cruise Phase:

For the interplanetary return phase of the mission, there were no specific trajectories described, and no recent NASA Mars missions to model this. A simple Hohman transfer was again used to describe the state vectors over the return trip. States were sampled in 1 day time increments over 8.5 months.

Figure 4-14 is a plot of the cumulative cross sectional area flux of meteoroids 1 microgram or larger factored into 5 km/s closing speed bins for the Mars to Earth transit phase of the mission.

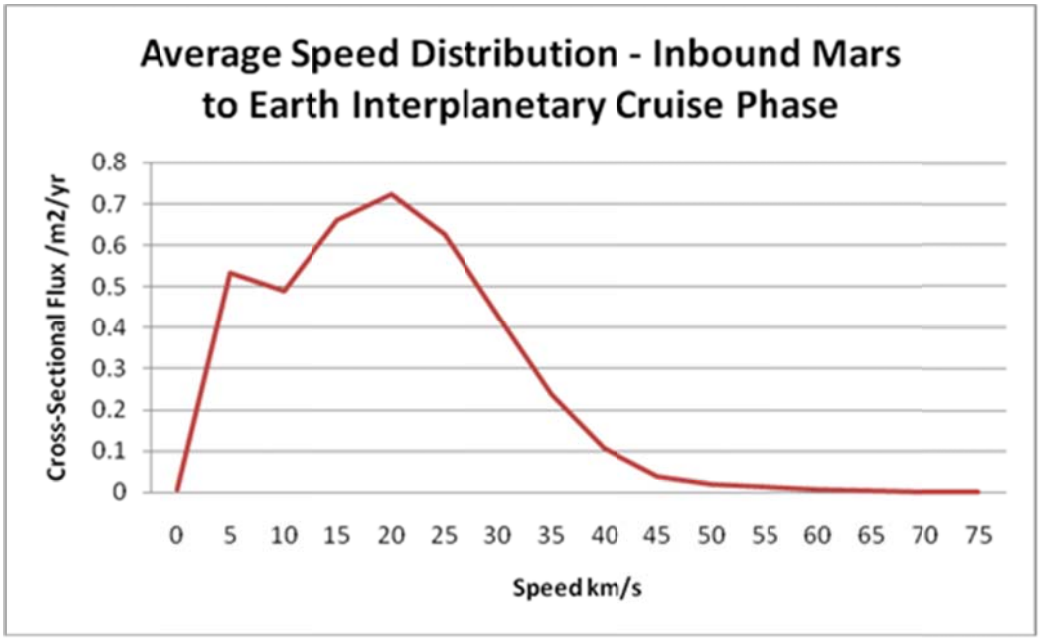

Figure 4-14. Average Speed Distribution over the inbound interplanetary cruise portion of the mission; generated using an average environment from the interplanetary cruises of a simple Hohman transfer orbit.

4.4.3.4 Meteoroid Environment Uncertainty

Currently there is insufficient data to construct an "uncertainty" for the meteoroid environment. The one sigma uncertainty files that were provided by the Meteoroid Environment Office describe the environmental differences between the orbits or flight paths and do not reflect actual uncertainty in the environment.

Earth to Mars transit phase – The Interplanetary Meteoroid Engineering Model (IPMEM v 2.1) was used to calculate an average meteoroid environment file over the interplanetary cruise phase for Spirit, Mars Reconnaissance Orbiter (MRO) and a simple Hohman transfer. These three missions represent different trajectories to Mars with varying transfer times. State vectors were selected using the same time step between each of their Earth departures and Mars arrivals. These three trajectories were analyzed separately and then averaged to produce the environment file. A 1 sigma variation was determined between the three different courses. The 1 sigma file can be added to or subtracted from the average interplanetary meteoroid file above to represent the variation in the meteoroid flux due to the unknown flight path

Aerobraking and Mars orbit phases – The Aerobraking and the Mars orbit one sigma uncertainty files were generated using the customary MEM procedure. MEM is a Monte Carlo code that, in this case, generated a flux estimate for 60 second segments of the orbit. The various segments were averaged together to obtain an average flux for the trajectory. The standard deviation was calculated from the same data set. All orbits have the same inclination and approximately the same node since no other information was given. The MEO also said that the one sigma files were meant to bound the variation in flux due to unknown orbit plane orientation.

Mars to Earth transit phase – The same uncertainty that was calculated from the outbound interplanetary cruise portion was used to develop the inbound sigma file. The one sigma standard deviation file for the Mars to Earth transit phase is intended to represent the variation in the meteoroid flux due to the unknown flight path.

4.5 Ballistic Limit Equations

4.5.1 SLA561V ablator BLE

The SLA-561V impact tests were performed on two specimens provided by the Stardust program. The ablator was 0.75 inches thick and was bonded to a 1.25 inch thick aluminum honeycomb. Specimen fabrication started with applying an adhesive film to the aluminum honeycomb face sheet. HRP F35-2.5 Flexcore was taped to the panels with J414 polyethylene tape to prevent it from moving. The assembly was then cured in an oven under an 8-inch Hg vacuum. The technicians then mixed a "wetcoat" of silicone resin, catalyst and solvent and the Super-Light Ablator SLA-561V. (The SLA material is composed of a silicone resin, catalyst, glass and cork fillers and has a bulk density of 0.257 g/cm^3 when cured). The test panels were then sprayed with DC-1200 silane primer. The wet coat was then sprayed onto the test panels. The mixed Super-Light Ablator (SLA-561V) was hand applied to fill the Flexcore cells. The test articles were then vacuum bagged, and heat cured. The tops of the core cells were machined flat.

The test results are listed in Table 4-7. The first column lists the projectile and target materials. The second column lists the projectile diameter in cm. The third column lists the impact speed in km/s. The fourth column list the impact angle in degrees measured from the target normal. The fifth column lists the measured crater depth in cm. The sixth column lists the impact speed pi-group, the seventh column lists the crater depth pi-group. The last column lists the shot number.

Table 4-7. SLA561V Hypervelocity Impact Test Results.

	d (cm)	U (km/s)	β (deg)	P (cm)	$d^{1/18}\,\delta^{0.5}\,(V\cos\beta)^{2/3}$	P/d	Shot no.
Nylon->SLA	0.318	6.00	70	1.905	3.536322	6.0	A-2552
2017-T4->SLA	0.060	6.83	0	0.670	10.12642	11.2	HITF07001
2017-T4->SLA	0.100	6.81	60	0.784	6.550056	7.8	HITF07002
2017-T4->SLA	0.100	6.88	45	0.928	8.309009	9.3	HITF07003
2017-T4->SLA	0.110	6.93	0	1.694	10.57520	15.4	HITF07004

Test A-2552 was performed in 1995 and the results are documented in (Gabriel and Christiansen, 1996). Four tests were performed on the second test article in 2007. The results of the second series of tests were document in (Lyons, 2007). Figure 4-15 is a photograph of the second test article after the Orion program had performed 4 hypervelocity impact tests.

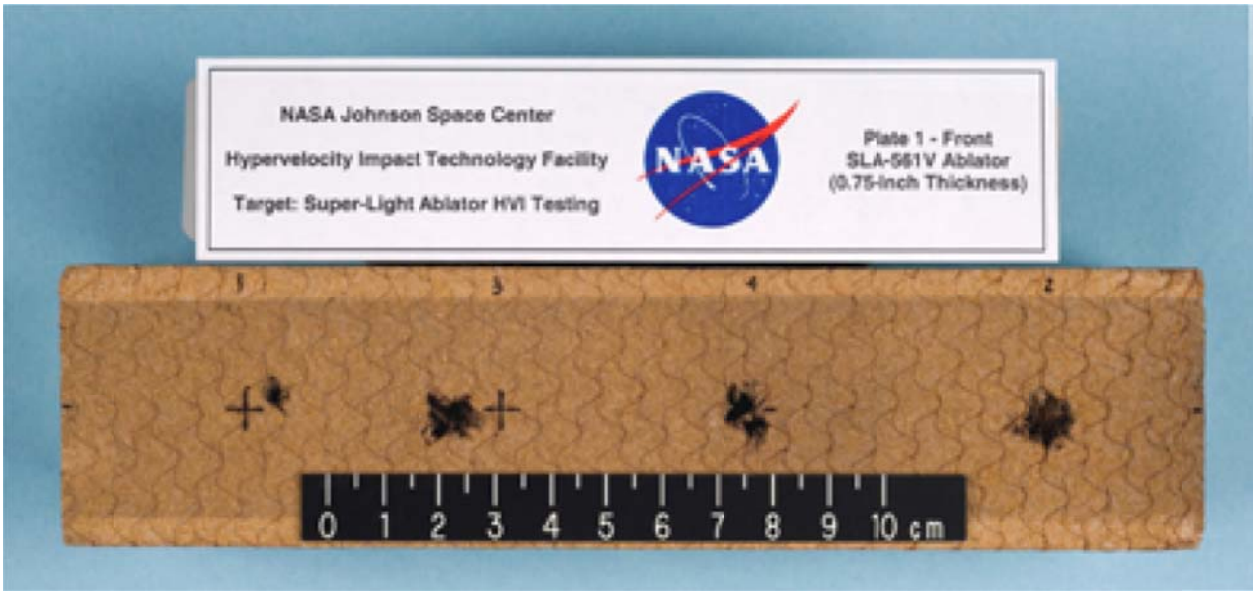

Figure 4-15. Second SLA561V Test Article at the Completion of Testing.

The 1995 test point was fitted with the equation

$$\frac{P}{d} = 3.7\, d^{1/18}\, \delta^{0.5}\, (V\, cos\beta)^{2/3}$$

reported in (Lyons, 2007), where P is the crater depth in cm, d is the projectile diameter in cm, δ is the projectile diameter in g/cm^3, V is the impact speed in km/s and β is the impact angle measured from the target normal.

This equation was coded up in BUMPER during November 2006 and was used for the aft TPS penetration analysis. The BLE and the test data are cross-plotted in Figure 4-16.

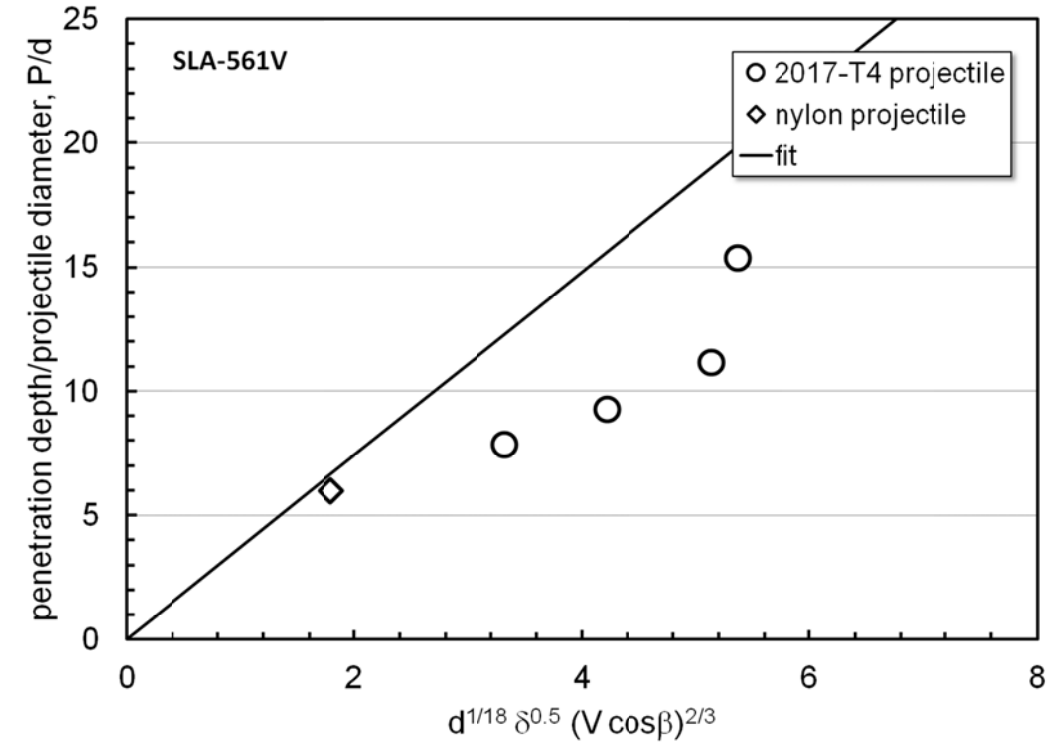

Figure 4-16. Scaled SLA561V Crater Depth as a Function of Scaled Impact Speed.

The failure criterion for the aft TPS was assumed to be a crater with depth equal to the 1.0 cm thickness of the aft TPS SLA561V. The diameter of the aluminum orbital debris particle that will penetrate to 1.0 cm is plotted in Figure 4-17.

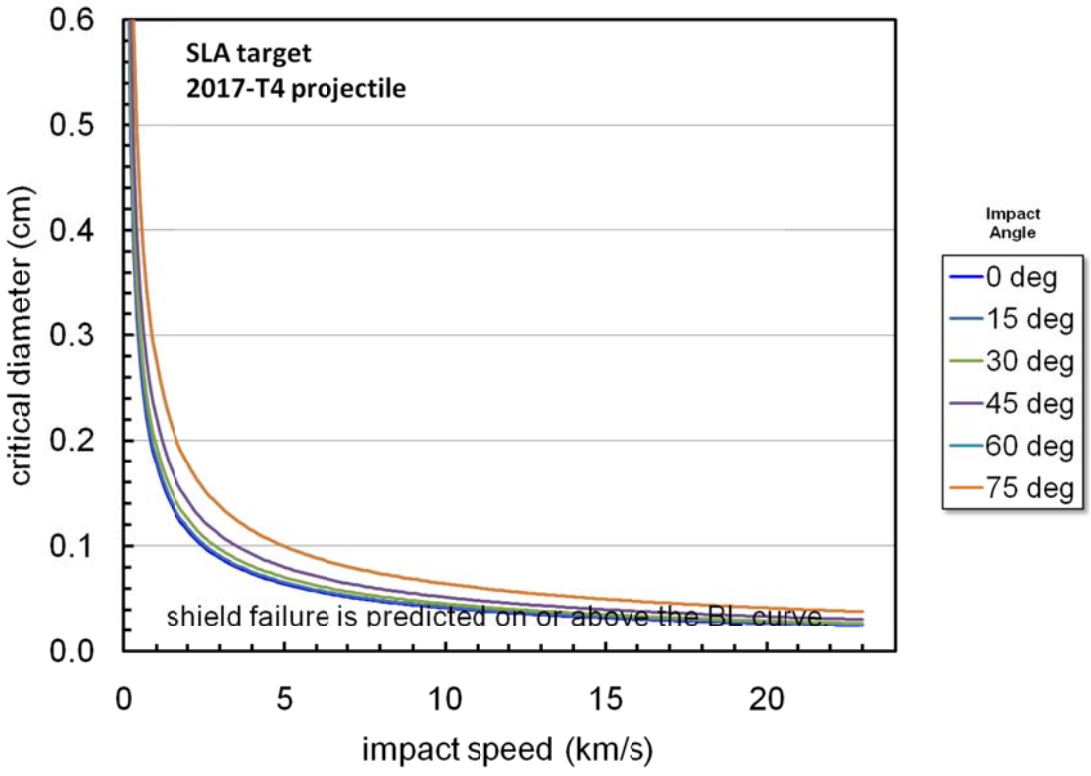

Figure 4-17. Orbital Debris Ballistic Limit Curve for 1.0 cm Deep Craters in Semi-Infinite SLA561V Targets.

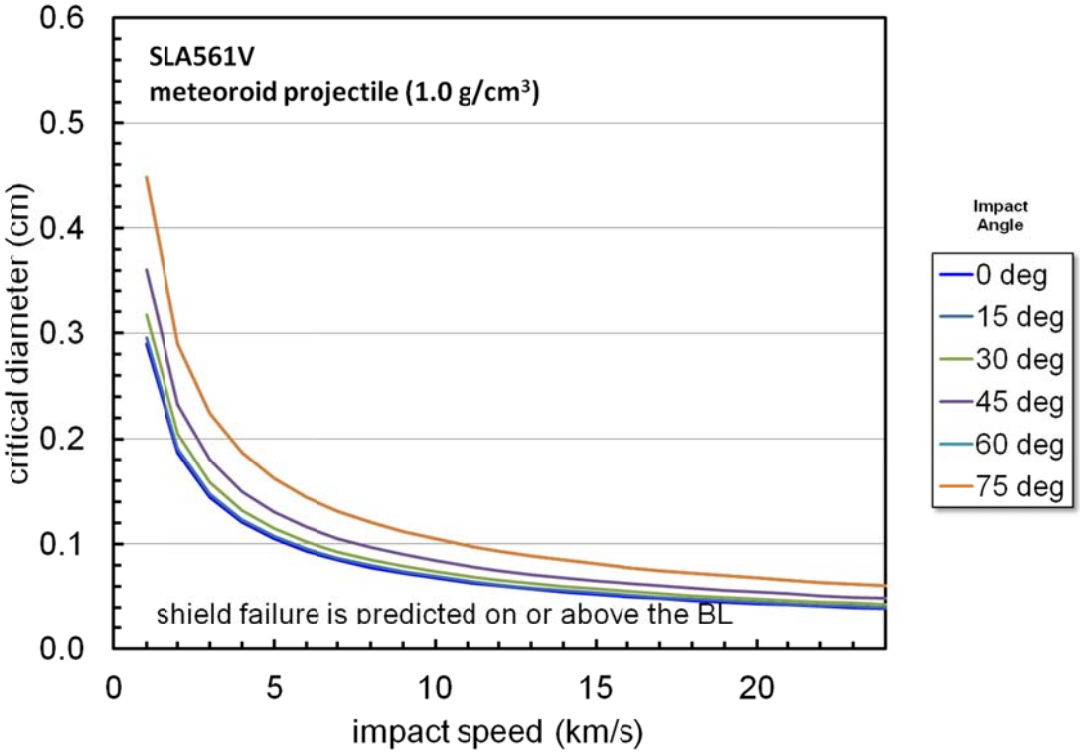

Figure 4-18 Meteoroid Ballistic Limit Curve for 1.0 cm Deep Craters in Semi-Infinite SLA561V Targets.

4.5.2 Carbon Phenolic BLE

The carbon phenolic BLE was developed for this report from a Naval Research Laboratory report (Halperson, 1968), available from the Defense Technical Information Center, and from two tests performed by NASA for the Orion program (Hedman, 2007).

Material characterization data were not readily apparent in the NRL reports. What was found is reproduced in Table 4-8.

Table 4-8. Target and projectile material properties.

	Density (g/cm^3)	UTS (KSI)	Sound speed (km/s)
Carbon Phenolic, NRL	1.49	15	3.7
Carbon Phenolic, Orion	1.48	3	…
glass	2.50		

The glass projectile mass density was calculated from the nominal 1/8 inch diameter of the glass sphere projectiles and the reported projectile masses. (Variation in the nominal diameter of the spheres resulted in calculated densities ranging from 2.2 to 2.7 g/cm^3, with the average around 2.5 g/cm^3. A 2.5 g/cm^3 density indicates the projectiles were made of soda lime glass.) Reports prior to the one referenced mentioned testing carbon tape phenolic and chopped carbon tape phenolic. No mention was made in the referenced report which material was tested. However, a prior report mentioned that chopping the tape had more of an effect on the front surface spall than on the through hole diameter(Anon., 1963).

A search of MATWEB was performed as a check on the Carbon Phenolic material properties listed in Table 4-8. The search[1] obtained a range of mass densities from 1.31 to 1.44 g/cm^3 and a range of ultimate tensile strengths from 7.3 to 19 ksi, hence the values listed in Table 4-8 are within the range of possibilities.

[1] http://www.matweb.com/search/DataSheet.aspx?MatGUID=bdd98b907c6f4695b6578b12efbd1321&ckck=1

The Carbon Phenolic test data extracted from the NRL report and the JSC test data are reproduced in Table 4-9. The first column lists the projectile and target materials. The second column lists the projectile diameter in cm, the third column lists the impact speed in km/s, the fourth column lists the crater depth in cm, the fifth column lists the impact angle in degrees measured from the target normal. The sixth and seventh columns list the pi-groups used to scale the impact speed and the crater depth respectively. The eighth column lists the page or figure number were the data were taken from in the NRL report.

Table 4-9. 1/8 inch Glass and 3/16 inch Aluminum Spheres Impacting Carbon Phenolic.

Projectile->target	D (cm)	U (km/s)	P (cm)	β (deg)	$V/\sqrt{(Y/\rho)}\,(\rho/\delta)^{-0.727}$	P/d	source
Glass->CP	0.318	0.85	0.143591	0	4.706248	0.451545	scaled from Figure 6
Glass->CP	0.318	4.63	0.861549	0	25.57744	2.709273	scaled from Figure 6
Glass->CP	0.318	6.18	0.963574	0	34.17146	3.030108	scaled from Figure 6
Glass->CP	0.318	6.66	0.967353	0	36.83151	3.041991	scaled from Figure 6
Glass->CP	0.318	8.03	1.073157	0	44.40243	3.374708	scaled from Figure 6
Glass->CP	0.318	8.18	1.031591	0	45.22091	3.243998	scaled from Figure 6
Glass->CP	0.318	5.76	0.842655	45	22.50814	2.649859	scaled from Figure 6
2017->CP	0.477	6.81	1.09400	45	27.42584	2.293501	HITF10172
2017->CP	0.421	6.77	1.07000	30	40.89712	2.541568	HITF10173

The extra parameters in the column 6 pi-group are the target mass density ρ and the projectile mass density δ.

The last two lines of Table 4-9 are the JSC data. These data were collected in 2010 and use an Orion Carbon Phenolic candidate material. The Carbon Phenolic was described in the test plan as:

> A structural carbon/phenolic composite pad provided by NASA Langley Research Center. The targets are machined to a 1" thick disk that is 9.5" in diameter. The carbon/phenolic pad has a density of approximately 92.3 lb/ft^3 (1.48 g/cm^3). The ply normal vector has an approximate 20° orientation with respect to the disk normal vector. The through-thickness Young's modulus, shear modulus and tensile strength are approximately 2.6 Msi (18 GPa), 0.9 Msi (6 GPa) and 3 ksi (20 MPa), respectively.

The ultimate tensile strength (UTS) of the Langley Carbon Phenolic given above is 1/5 the UTS of the NRL material.

The JSC test article post test is shown in Figure 4-19.The impacts at the 3 O'clock and the 9 O'clock positions were aimed near the edge to cause edge breakout. These tests are not reported here. The tests at the 12 O'clock and the 6 O'clock positions are HITF1072 and HITF1073, respectively.

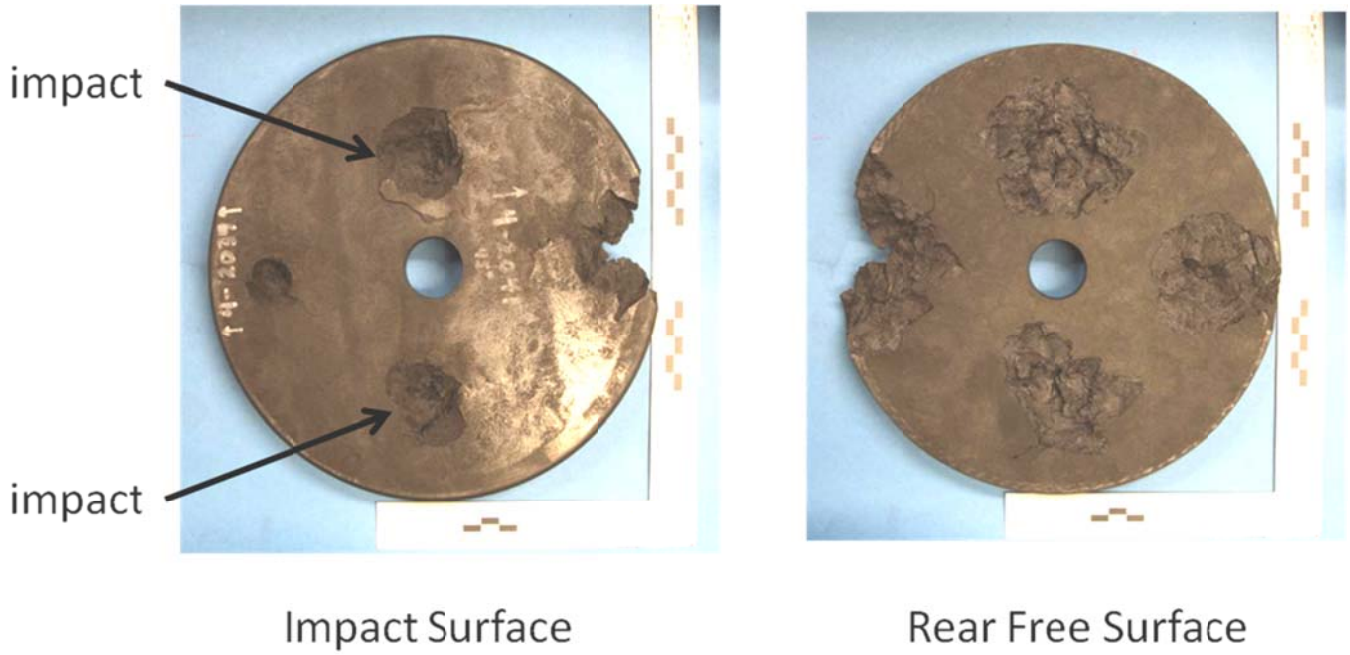

Figure 4-19. Post Test Views of the JSC Test Article.

Rear free surface spall in metals usually means that the crater depth in the finite thickness target is larger than the crater depth in a semi-infinite target for similar impact conditions.

A close-up of the HITF1072 impact side crater is shown in Figure 4-20.

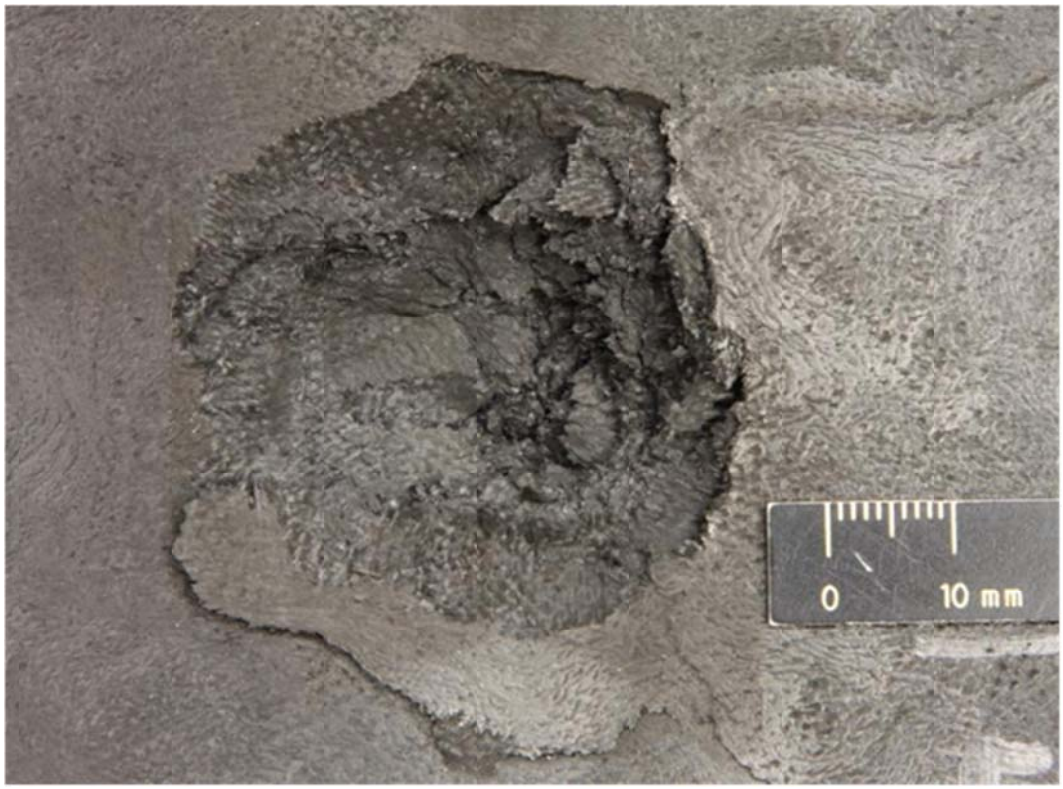

Figure 4-20. HITF 1072 Impact Side Crater.

The Carbon Phenolic data were scaled using pi-groups developed for metals cratering. The results are plotted in Figure 4-21. The metals scaling relation is plotted as the dashed curve. This curve applies to the crater depth in metals in the large impact

speed limit. There are reasons for thinking that Carbon Phenolic will follow the metals scaling relation at large impact speeds, however, the shock impedance mismatch between the projectile and target materials could preclude this from happening in the testable range of impact speeds. For aluminum projectiles striking aluminum targets the large speed limit the dashed curve applies to is 3 km/s and larger. However, if there is a large shock impedance mismatch between the projectile and the target, then the large speed limit could be at even larger speeds. For example, for nylon striking aluminum targets the large speed limit is 10 km/s and larger and for steel projectiles striking aluminum the large speed limit is 80 km/s and larger. The shock impedance of aluminum and glass is larger than the impedance of Carbon Phenolic so the authors expect the Carbon Phenolic hypervelocity impact data to lie above the metals crater depth scaling relation, which the NRL data do. However, the JSC data do not. This might indicate that for impact speeds less than the large speed limit the crater depth does not scale with the normal component of the impact velocity, like it does in the large speed limit. It might also indicate that there are material differences that are not captured by scaling with the UTS and the mass density. Further testing is required to establish a reliable method for extrapolating the crater depth data collected at testable impact speeds to impact speeds typical of meteoroids.

For this preliminary assessment of the risk of forward TPS perforation the authors took the expedient of extrapolating the test data to large impact speeds using the metals crater depth scaling relation renormalized to lie above all the Carbon Phenolic test data. The solid curve in Figure 4-21was the result.

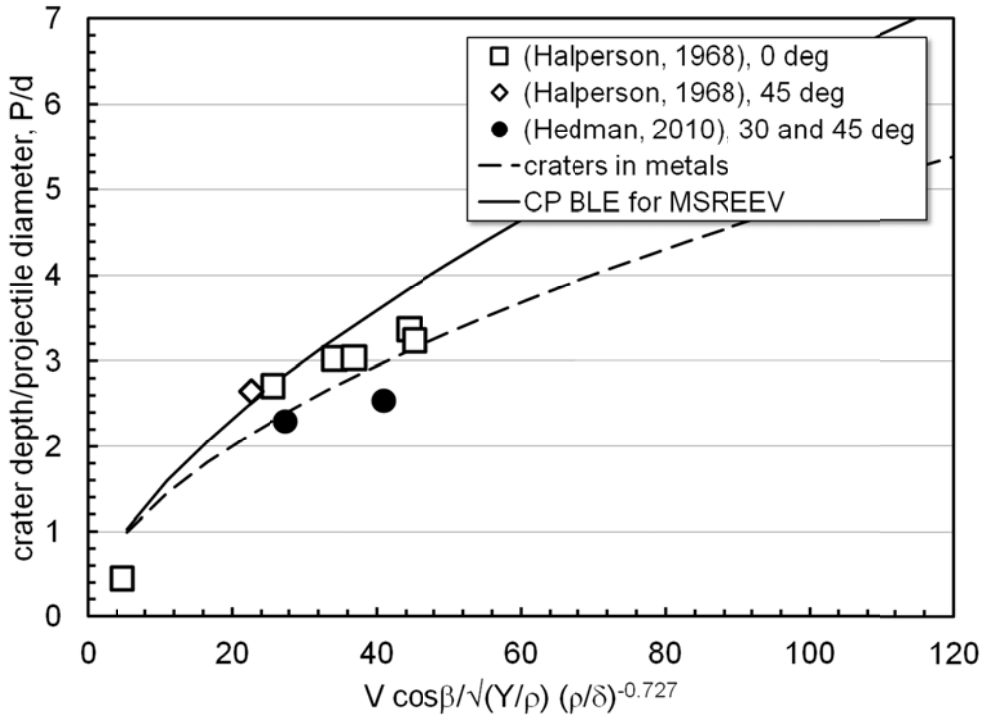

Figure 4-21. Scaled Carbon Phenolic Crater Depth as a Function of Scaled Impact Speed.

The solid curve in Figure 4-21 can be simplified to the following equation for Carbon Phenolic,

$$\frac{P}{d} = 0.60885\, d^{1/18}\, \delta^{1/2} (V \cos\beta)^{2/3}$$

where P is the crater depth in cm, d is the projectile diameter in cm, δ is the projectile diameter in g/cm^3, V is the impact speed in km/s and β is the impact angle measured from the target normal. The above equation applies to the high strength material properties listed in Table 4-8 for the NRL carbon phenolic.

The failure criterion for the forward TPS was assumed to be a crater with depth equal to the 1.2 cm thickness of the forward TPS Carbon Phenolic. The diameter of the aluminum orbital debris particle that will penetrate to 1.2 cm is plotted in Figure 4-22. The SLA561V BLE, plotted in Figure 4-17, and the Carbon Phenolic BLE, plotted in Figure 4-22, are plotted on the same scale. About a 6.5 times larger orbital debris particle is required to fail the forward TPS compared to the aft TPS, at 7 km/s impact speed. The small size particles that lead to aft TPS failure are the reason why the aft TPS failure dominates the MMOD reliability of the MSREEV.

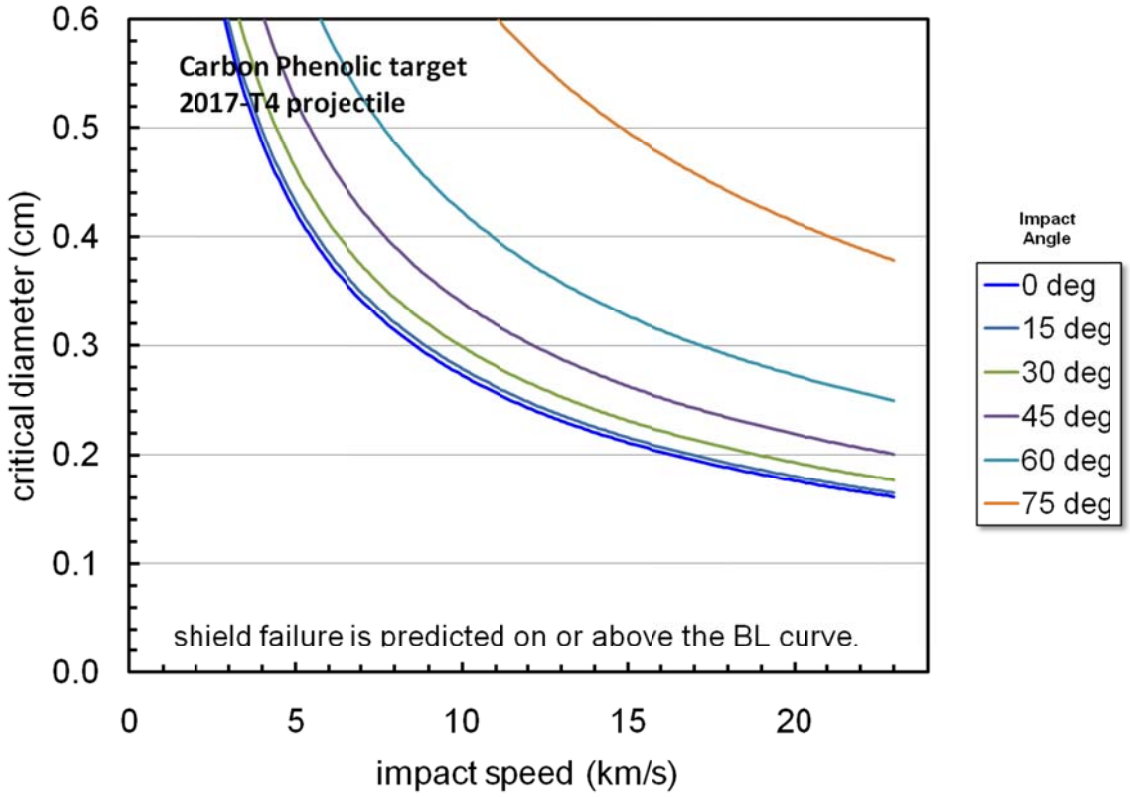

Figure 4-22. Orbital Debris Ballistic Limit Curve for 1.2 cm Deep Craters in Semi-Infinite Carbon Phenolic Targets.

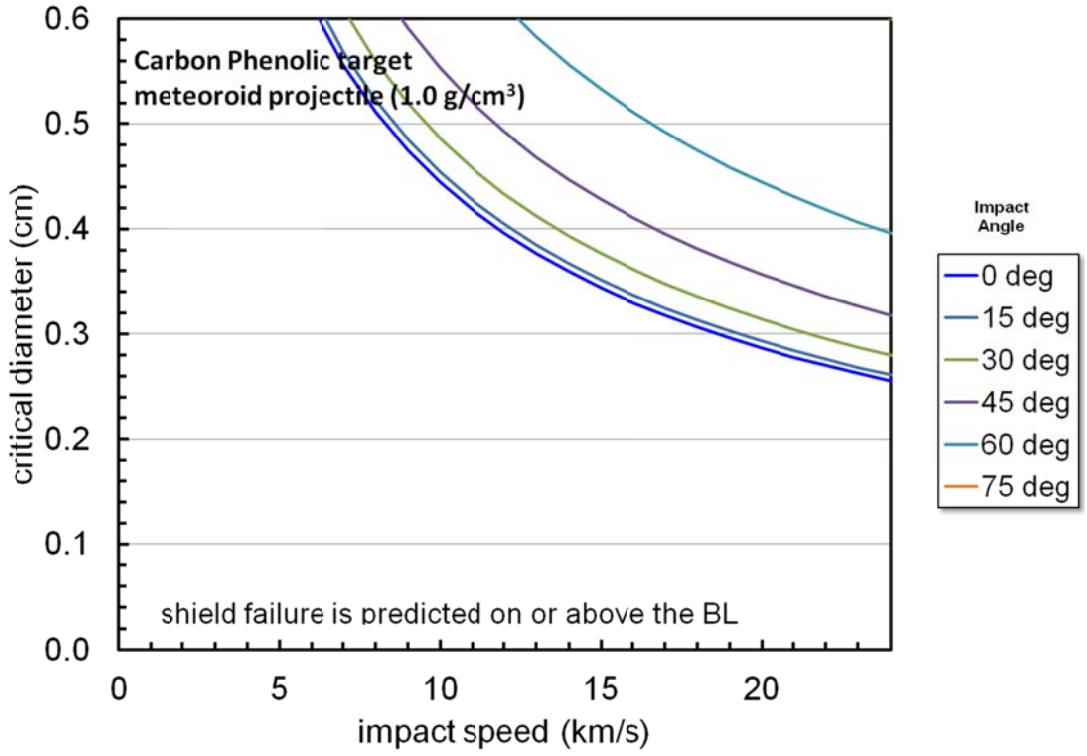

Figure 4-23 Meteoroid Ballistic Limit Curve for 1.2 cm Deep Craters in Semi-Infinite Carbon Phenolic Targets.

4.5.3 Multi-Shock Shield BLE

The MMOD "garage" shield shown in Figure 4-5 was analyzed with an advanced Nextel Multi-Shock shield that was developed at the NASA Johnson Space Center Hypervelocity Impact Technology Facility (HIT-F) (Christiansen, 1993). Of the three available configurations, only #2 was available in the Bumper code at the time of the analysis:

1. Four equally spaced ceramic fabric bumpers with a flexible rear wall
2. Four equally spaced ceramic bumpers with an aluminum rear wall
3. Two equally spaced ceramic bumpers with a two-sheet aluminum Whipple shield

The MMOD Shield Ballistic Limit Analysis program (Ryan and Christiansen, 2010) was used to size a shield that would protect against a 10 mm diameter meteoroid particle with a density of 1 g/cc and a velocity of 25 km/s impacting at 0 degrees. The shielding design assumed a total shield stand-off distance of 30 cm, with three Nextel layers (total areal density = 0.19 g/cm^2) equally spaced at 7.5 cm. The rear wall of the shield was a 0.18 cm 2219-T87 aluminum sheet (areal density = 0.51 g/cm^2) at a distance of 7.5 cm from the closest Nextel layer. The total areal density of this design was 0.698 g/cm^2

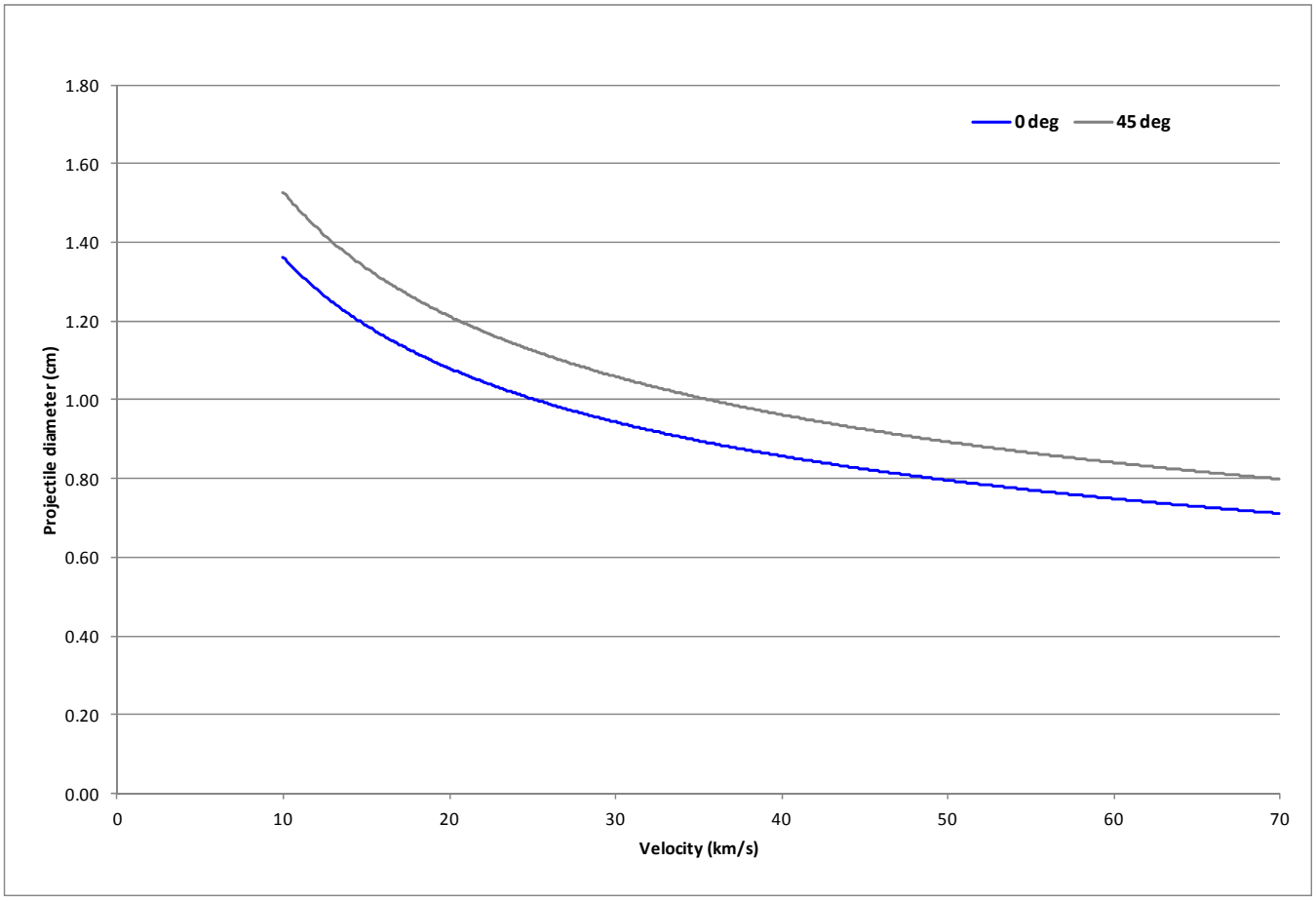

Figure 4-24. 0° and 45° Ballistic Limit Curves for Nextel Multi Shock "Garage" Shield Concept sized to protect against a 1 cm meteoroid projectile at 25 km/s. Shield failure (detached spall) is predicted for particle diameters above the curves.

5. Results

Three different studies were performed. First was a calculation of the risk of MMOD impact as a function of impact speed and impact angle. Second was a calculation of the probability of TPS failure. Third, and last, was the evaluation of an MMOD shield concept for protecting the EEV from meteoroid impact.

5.1 MSR EEV Impact Analysis Results

The impact analysis task produced tables of fluxes for discrete ranges of impact speed and impact angle. The impact speed is indexed by the row number and the impact angle is indexed by the column number. Tables were calculated for the forward and aft TPS, all 24 attitudes, mission phases 2 through 14, and four meteoroid diameters, for a total of 2,496 tables. Also, each mission phase was averaged over all 24 attitudes to produce an additional 104 tables. The four meteoroid diameters used to construct the tables are 1 mm, 100 microns, 50 microns, and 10 microns.

Table 5-1 is the table of fluxes of meteoroids 1 mm or larger impacting on the forward TPS in Mars orbit. The first column of numbers is the row number. For the meteoroid tables, the first row corresponds to impact speeds from 0 to 5 km/s, the second to impact speeds from 5 to 10 km/s, the third to 10 to 15 km/s, … to 95 to 100 km/s. The second column of numbers are the numbers of impacts onto the forward TPS during 1 year which strike the forward TPS at angles between 0 to 10 degrees measured with respect to the TPS normal. The third column is for impacts between 10 and 20 degrees, the fourth for impacts between 20 to 30 degrees, etc.

Table 5-1 Table of Fluxes of 1 mm or Larger Meteoroids on the Forward TPS During the Mars Orbit Phase. See the text for a description of the table format.

1	0.287641E-09	0.196118E-08	0.472333E-08	0.100505E-07	0.212162E-07	0.358120E-07	0.426525E-07	0.399513E-07	0.328257E-07
2	0.303743E-07	0.207193E-06	0.500482E-06	0.106801E-05	0.224398E-05	0.386765E-05	0.468660E-05	0.452362E-05	0.403417E-05
3	0.121643E-06	0.833632E-06	0.203099E-05	0.440456E-05	0.934275E-05	0.161477E-04	0.195205E-04	0.189005E-04	0.170512E-04
4	0.160867E-06	0.110365E-05	0.270271E-05	0.591127E-05	0.126135E-04	0.218788E-04	0.263875E-04	0.255317E-04	0.231884E-04
5	0.154255E-06	0.106028E-05	0.261649E-05	0.579650E-05	0.123435E-04	0.214674E-04	0.259225E-04	0.252382E-04	0.235479E-04
6	0.108287E-06	0.745538E-06	0.184463E-05	0.413211E-05	0.877512E-05	0.152294E-04	0.183810E-04	0.179461E-04	0.169071E-04
7	0.457404E-07	0.314093E-06	0.770914E-06	0.171648E-05	0.366298E-05	0.629008E-05	0.750787E-05	0.720792E-05	0.653339E-05
8	0.113043E-07	0.766296E-07	0.184142E-06	0.390487E-06	0.841964E-06	0.141810E-05	0.167130E-05	0.156160E-05	0.130640E-05
9	0.503045E-08	0.331307E-07	0.772979E-07	0.156012E-06	0.332641E-06	0.558328E-06	0.667963E-06	0.629812E-06	0.524140E-06
10	0.361101E-08	0.236600E-07	0.549437E-07	0.109572E-06	0.233372E-06	0.391691E-06	0.468447E-06	0.439367E-06	0.362316E-06
11	0.186309E-08	0.121913E-07	0.282336E-07	0.555687E-07	0.118714E-06	0.200323E-06	0.240340E-06	0.225617E-06	0.186759E-06
12	0.328930E-09	0.211381E-08	0.478186E-08	0.889562E-08	0.191588E-07	0.324598E-07	0.388128E-07	0.354117E-07	0.278238E-07
13	0.987958E-13	0.613366E-12	0.135132E-11	0.242919E-11	0.513771E-11	0.844377E-11	0.986245E-11	0.833185E-11	0.541767E-11
14	0.000000E+00	0.000000E+00	0.000000E+00	0.000000E+00	0.000000E+00	0.000000E+00	0.000000E+00	0.000000E+00	0.000000E+00
15	0.000000E+00	0.000000E+00	0.000000E+00	0.000000E+00	0.000000E+00	0.000000E+00	0.000000E+00	0.000000E+00	0.000000E+00
16	0.000000E+00	0.000000E+00	0.000000E+00	0.000000E+00	0.000000E+00	0.000000E+00	0.000000E+00	0.000000E+00	0.000000E+00
17	0.000000E+00	0.000000E+00	0.000000E+00	0.000000E+00	0.000000E+00	0.000000E+00	0.000000E+00	0.000000E+00	0.000000E+00
18	0.000000E+00	0.000000E+00	0.000000E+00	0.000000E+00	0.000000E+00	0.000000E+00	0.000000E+00	0.000000E+00	0.000000E+00
19	0.000000E+00	0.000000E+00	0.000000E+00	0.000000E+00	0.000000E+00	0.000000E+00	0.000000E+00	0.000000E+00	0.000000E+00
20	0.000000E+00	0.000000E+00	0.000000E+00	0.000000E+00	0.000000E+00	0.000000E+00	0.000000E+00	0.000000E+00	0.000000E+00

One has to multiply Table 5-1 by the duration of exposure in years listed in Table 4-3 for the Mars orbit mission phase to obtain a number of impacts. Table 4-3 lists 3 years of exposure for the Mars Orbit phase, so one must multiply the fluxes in Table 4-3 by 3 to obtain the numbers of impact. If the Mars orbit phase is lengthened or shortened, then one would multiply by the new exposure duration.

The first ten rows of Table 5-1 are plotted as a 3D column chart in Figure 5-1. These plots are called V-β plots at JSC/KX because impact speed is usually denoted as V and impact angle as β. The plot shows that randomizing the EEV attitude has smeared out the number of impacts over a broad range of impact angles.

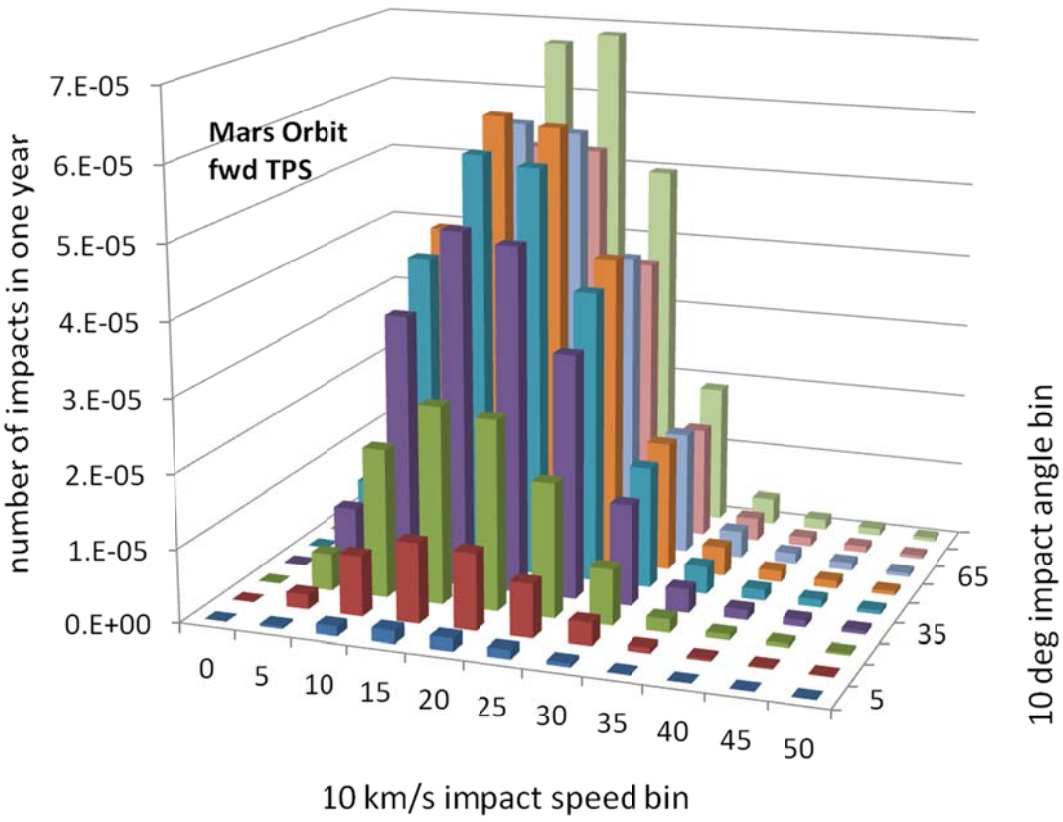

Figure 5-1 v-β Plot for the Forward TPS in Mars Orbit.

The tables for the flux of orbital debris particles were treated differently. First only one attitude was used, the 20 degrees entry angle shown in Figure 4-7. Second only one mission phase was analyzed, mission phase 15 Earth entry. Mission phase 1, launch to LEO, was not analyzed. This gives a total of 4 tables for the orbital debris analysis of the forward TPS, one for the 1 mm OD particles, one for the 100 micron diameter particles, one for the 50 micron diameter particles and one for the 10 micron diameter particles, and 4 tables for the aft TPS, for a total of 8 tables.

The orbital debris tables also differ from the meteoroid tables by the speed increment used for each row. The orbital debris tables have 20 rows, just like the meteoroid tables, and the row number is listed in the first column, just like the meteoroid tables, but row 1 corresponds to 0 to 1 km/s, row 2 to 1 to 2 km/s, …, row 20 to 19 to 20 km/s

The average attitude V-β tables for each mission phase were multiplied the duration of exposure listed in Table 4-3, summed over impact speed and angle, summed over both sides of the EEV, and then summed over the 15 mission phases to obtain a total number of impacts for each of the 4 particle sizes analyzed. The results are shown in Table 5-2 broken out by orbital debris particle impacts and by meteoroid impacts.

Table 5-2. MSR EEV Analysis - MMOD Impact Study Results Summary.

Number of Impacts - per Limiting Particle Size												
	0.1 cm			0.05 cm			0.01 cm			0.001 cm		
Attitude	OD	MM	Total	OD	MM	Total	OD	MM	Total	OD	MM	Total
1	6.78E-06	7.54E-04	7.60E-04	9.00E-05	1.22E-02	1.23E-02	5.40E-03	7.89E+00	7.90E+00	1.24E-01	8.26E+04	8.26E+04
2	6.78E-06	7.13E-04	7.20E-04	9.00E-05	1.16E-02	1.17E-02	5.40E-03	7.47E+00	7.47E+00	1.24E-01	7.82E+04	7.82E+04
3	6.78E-06	4.97E-04	5.03E-04	9.00E-05	8.06E-03	8.15E-03	5.40E-03	5.20E+00	5.21E+00	1.24E-01	5.45E+04	5.45E+04
4	6.78E-06	5.62E-04	5.69E-04	9.00E-05	9.12E-03	9.21E-03	5.40E-03	5.89E+00	5.89E+00	1.24E-01	6.16E+04	6.17E+04
5	6.78E-06	4.90E-04	4.96E-04	9.00E-05	7.94E-03	8.03E-03	5.40E-03	5.13E+00	5.13E+00	1.24E-01	5.37E+04	5.37E+04
6	6.78E-06	6.70E-04	6.76E-04	9.00E-05	1.09E-02	1.10E-02	5.40E-03	7.01E+00	7.02E+00	1.24E-01	7.34E+04	7.34E+04
7	6.78E-06	6.93E-04	6.99E-04	9.00E-05	1.12E-02	1.13E-02	5.40E-03	7.25E+00	7.26E+00	1.24E-01	7.60E+04	7.60E+04
8	6.78E-06	5.57E-04	5.64E-04	9.00E-05	9.04E-03	9.13E-03	5.40E-03	5.83E+00	5.84E+00	1.24E-01	6.11E+04	6.11E+04
9	6.78E-06	6.34E-04	6.40E-04	9.00E-05	1.03E-02	1.04E-02	5.40E-03	6.63E+00	6.64E+00	1.24E-01	6.95E+04	6.95E+04
10	6.78E-06	6.87E-04	6.94E-04	9.00E-05	1.11E-02	1.12E-02	5.40E-03	7.19E+00	7.20E+00	1.24E-01	7.53E+04	7.53E+04
11	6.78E-06	7.19E-04	7.26E-04	9.00E-05	1.17E-02	1.18E-02	5.40E-03	7.53E+00	7.53E+00	1.24E-01	7.88E+04	7.88E+04
12	6.78E-06	7.29E-04	7.35E-04	9.00E-05	1.18E-02	1.19E-02	5.40E-03	7.63E+00	7.64E+00	1.24E-01	7.99E+04	7.99E+04
13	6.78E-06	5.44E-04	5.51E-04	9.00E-05	8.82E-03	8.91E-03	5.40E-03	5.70E+00	5.70E+00	1.24E-01	5.96E+04	5.96E+04
14	6.78E-06	5.75E-04	5.81E-04	9.00E-05	9.32E-03	9.41E-03	5.40E-03	6.02E+00	6.02E+00	1.24E-01	6.30E+04	6.30E+04
15	6.78E-06	5.11E-04	5.17E-04	9.00E-05	8.28E-03	8.37E-03	5.40E-03	5.35E+00	5.35E+00	1.24E-01	5.60E+04	5.60E+04
16	6.78E-06	5.67E-04	5.74E-04	9.00E-05	9.20E-03	9.29E-03	5.40E-03	5.94E+00	5.94E+00	1.24E-01	6.22E+04	6.22E+04
17	6.78E-06	6.39E-04	6.46E-04	9.00E-05	1.04E-02	1.05E-02	5.40E-03	6.70E+00	6.70E+00	1.24E-01	7.01E+04	7.01E+04
18	6.78E-06	4.77E-04	4.84E-04	9.00E-05	7.74E-03	7.83E-03	5.40E-03	5.00E+00	5.00E+00	1.24E-01	5.23E+04	5.23E+04
19	6.78E-06	5.76E-04	5.83E-04	9.00E-05	9.35E-03	9.44E-03	5.40E-03	6.04E+00	6.04E+00	1.24E-01	6.32E+04	6.32E+04
20	6.78E-06	7.94E-04	8.01E-04	9.00E-05	1.29E-02	1.30E-02	5.40E-03	8.31E+00	8.32E+00	1.24E-01	8.70E+04	8.70E+04
21	6.78E-06	7.54E-04	7.60E-04	9.00E-05	1.22E-02	1.23E-02	5.40E-03	7.89E+00	7.90E+00	1.24E-01	8.26E+04	8.26E+04
22	6.78E-06	4.87E-04	4.93E-04	9.00E-05	7.89E-03	7.98E-03	5.40E-03	5.10E+00	5.10E+00	1.24E-01	5.34E+04	5.34E+04
23	6.78E-06	5.20E-04	5.27E-04	9.00E-05	8.44E-03	8.53E-03	5.40E-03	5.45E+00	5.45E+00	1.24E-01	5.70E+04	5.70E+04
24	6.78E-06	7.28E-04	7.35E-04	9.00E-05	1.18E-02	1.19E-02	5.40E-03	7.62E+00	7.63E+00	1.24E-01	7.98E+04	7.98E+04
	1.0 mm (1000 μm)			0.5 mm (500 μm)			0.1 mm (100 μm)			0.01 mm (10 μm)		
max	6.78E-06	7.94E-04	8.01E-04	9.00E-05	1.29E-02	1.30E-02	5.40E-03	8.31E+00	8.32E+00	1.24E-01	8.70E+04	8.70E+04
average	6.78E-06	6.20E-04	6.27E-04	9.00E-05	1.01E-02	1.01E-02	5.40E-03	6.49E+00	6.49E+00	1.24E-01	6.80E+04	6.80E+04
min	6.78E-06	4.77E-04	4.84E-04	9.00E-05	7.74E-03	7.83E-03	5.40E-03	5.00E+00	5.00E+00	1.24E-01	5.23E+04	5.23E+04

The second from the bottom row lists the number of impacts averaged over all 24 attitudes and all 15 mission phases, i.e., the average of the column of 24 numbers above it. The third row from the bottom lists the maximum of the column of 24 numbers and is representative of the mean number of impacts when in a "worst" case attitude. The last row lists the minimum of the column of 24 numbers and is representative of the mean number of impacts when in a "best" case attitude.

Note that the number of orbital debris impacts relative to the number of meteoroid impacts increases with the size of the particle. The 10 micron orbital debris particles impacts are 0.000119% of the 10 micron meteoroid impacts, 0.0684% of the 50 micron size particle impacts, 0.57% of the 100 micron size particle impacts and 0.63% of the 1 mm size particle impacts. However, in every case it is a significantly smaller number than the number of meteoroid impacts.

5.1.1 1.0 mm Impact Results

The results for the MSR EEV impact study for a limiting particle size of 1.0 mm are shown in Table 5-3. The results are broken out for each mission phase as well as for the two MSR EEV TPS components (aft and forward).

Table 5-3. MSR EEV Analysis - Impact Study Results for 1.0 mm Limiting Particle Size.

MSR EEV Analysis – 1.0 mm Impact Results			
	Number of Impacts - per Limiting Particle Size		
Missions Phase	**Forward**	**Aft**	**Total**
Launch-LEO (not analyzed)	…	…	…
Earth to Mars Transit	1.29E-04	3.98E-05	1.69E-04
Mars Aerobraking	2.92E-05	9.07E-06	3.82E-05
Mars Orbit	1.93E-04	5.99E-05	2.53E-04
Mars to Earth Insert	4.02E-07	1.25E-07	5.27E-07
Mars to Earth Transit	1.22E-04	3.74E-05	1.59E-04

MSR EEV Analysis – 1.0 mm Impact Results			
	Number of Impacts - per Limiting Particle Size		
Missions Phase	Forward	Aft	Total
EEV Entry (OD only)	3.13E-06	3.66E-06	6.78E-06
Total	**4.77E-04**	**1.50E-04**	**6.26E-04**

5.1.2 0.5 mm Impact Results

The results for the MSR EEV impact study for a limiting particle size of 0.5 mm are shown in Table 5-3. The results are broken out for each mission phase as well as for the two MSR EEV TPS components (aft and forward).

Table 5-4. MSR EEV Analysis - Impact Study Results for 0.5 mm Limiting Particle Size.

MSR EEV Analysis – 0.5 mm Impact Results			
	Number of Impacts - per Limiting Particle Size		
Missions Phase	Forward	Aft	Total
Launch-LEO (not analyzed)	…	…	…
Earth to Mars Transit	2.10E-03	6.45E-04	2.74E-03
Mars Aerobraking	4.73E-04	1.47E-04	6.20E-04
Mars Orbit	3.13E-03	9.72E-04	4.10E-03
Mars to Earth Insert	6.53E-06	2.03E-06	8.56E-06
Mars to Earth Transit	1.97E-03	6.07E-04	2.58E-03
EEV Entry (OD only)	4.46E-05	4.55E-05	9.00E-05
Total	**7.72E-03**	**2.42E-03**	**1.00E-02**

5.1.3 0.1 mm Impact Results

The results for the MSR EEV impact study for a limiting particle size of 0.1 mm are shown in Table 5-5. The results are broken out for each mission phase as well as for the two MSR EEV TPS components (aft and forward).

Table 5-5. MSR EEV Analysis - Impact Study Results for 0.1 mm Limiting Particle Size.

MSR EEV Analysis – 0.1 mm Impact Results			
	Number of Impacts - per Limiting Particle Size		
Missions Phase	Forward	Aft	Total
Launch-LEO (not analyzed)	…	…	…
Earth to Mars Transit	1.35E+00	4.16E-01	1.77E+00
Mars Aerobraking	3.05E-01	9.49E-02	4.00E-01
Mars Orbit	2.02E+00	6.27E-01	2.65E+00
Mars to Earth Insert	4.21E-03	1.31E-03	5.52E-03
Mars to Earth Transit	1.27E+00	3.92E-01	1.67E+00
EEV Entry (OD only)	3.09E-03	2.31E-03	5.40E-03
Total	**4.95E+00**	**1.53E+00**	**6.50E+00**

5.1.4 0.01 mm Impact Results

The results for the MSR EEV impact study for a limiting particle size of 0.01 mm are shown in Table 5-6. The results are broken out for each mission phase as well as for the two MSR EEV TPS components (aft and forward).

Table 5-6. MSR EEV Analysis - Impact Study Results for 0.01 mm Limiting Particle Size.

MSR EEV Analysis – 0.01 mm Impact Results	
Missions Phase	Number of Impacts - per Limiting Particle Size

	Forward	Aft	Total
Launch-LEO (not analyzed)	…	…	…
Earth to Mars Transit	1.42E+04	4.36E+03	1.85E+04
Mars Aerobraking	3.20E+03	9.94E+02	4.19E+03
Mars Orbit	2.12E+04	6.57E+03	2.77E+04
Mars to Earth Insert	4.41E+01	1.37E+01	5.78E+01
Mars to Earth Transit	1.33E+04	4.10E+03	1.74E+04
EEV Entry (OD only)	7.25E-02	5.17E-02	1.24E-01
Total	**5.19E+04**	**1.60E+04**	**6.78E+04**

5.1.5 Metrics

The probability of meteoroid impact for a given diameter meteoroid or larger is plotted in Figure 5-2. The diameter meteoroid that impacts with a probability equal to the requirement, when the EEV is the lower risk attitude is 5.8 mm, and the diameter meteoroid that strikes with a probability equal to the higher risk attitude is 6.6 mm.

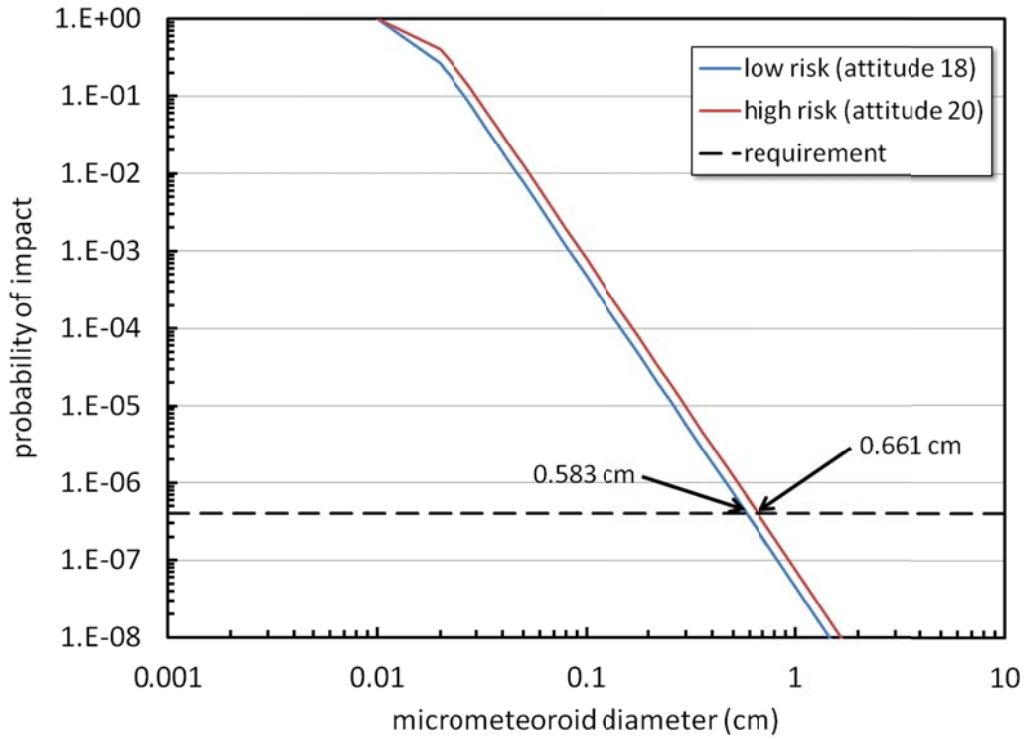

Figure 5-2 Diameter meteoroid that has a probability of 4×10^{-7} of impacting the EEV during 4.38 years.

The simple meteoroid power-law flux relation Eq. (1) means that if the number of impacts N_{ref} at reference diameter d_{ref}, that the number of impacts by meteoroids with diameter d or larger is

$$N(>d) = N_{ref}\left(\frac{d_{ref}}{d}\right)^{-4.02}$$

The fraction of meteoroid impacts that occur during mission phase are plotted in Figure 5-3. The part due to impacts on the forward TPS are plotted in red and the part that are due to impacts on the aft TPS are plotted in blue. The orbital debris cumulative flux relation is not a power-law, so number of orbital debris impacts cannot be cross plotted with the meteoroid results in Figure 5-3.

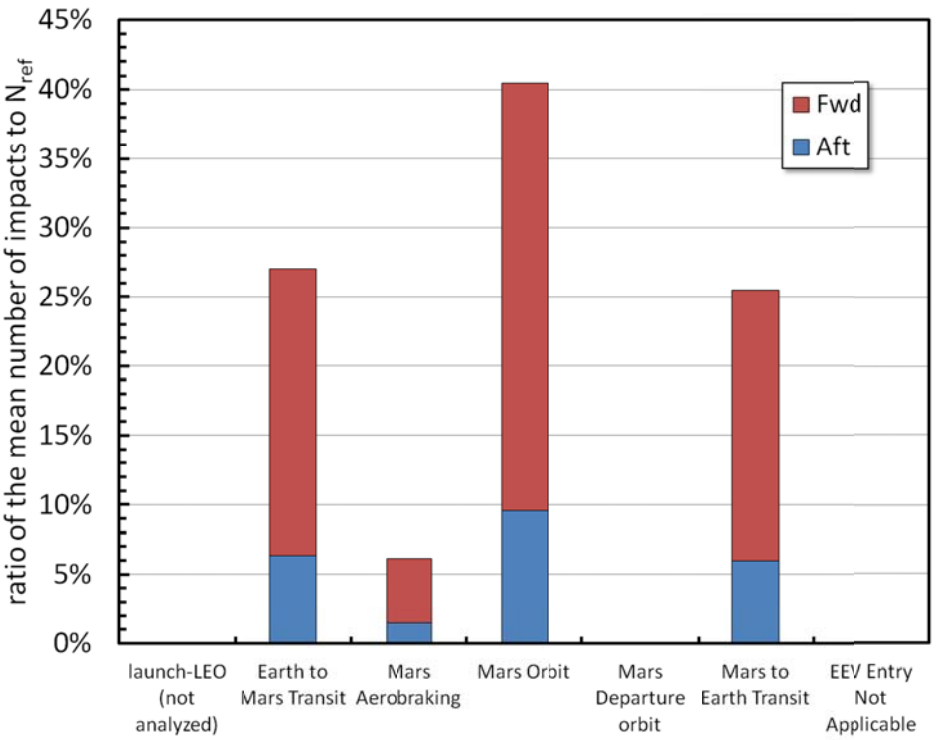

Figure 5-3 Fraction of meteoroid impacts at a given size as a function of mission phase and whether the impact was on the forward or aft TPS.

5.2 MSR EEV Probability of TPS Failure by MMOD Impact

Table 5-7. is a list of the results from a calculation of the probability of TPS failure by MMOD impact. The first column lists the mission phase, the second column lists the probability of an MMOD impact onto the forward TPS causing a TPS failure on Earth entry, the third column lists the probability of an MMOD impact onto the aft TPS causing a TPS failure on Earth entry and the fourth column is the probability of an impact on either the forward or aft TPS causing a TPS failure. All three columns are probabilities calculated by averaging over all 24 attitudes listed in Figure 4-6.

Table 5-7. MSR EEV Probability of TPS Failure Due to MMOD Impact.

MSR EEV TPS Failure by MMOD Impact			
	Probability of TPS Failure		
Missions Phase	Forward	Aft	Total
Launch-LEO (not analyzed)	…	…	…
Earth to Mars Transit	1.32E-06	5.53E-04	5.54E-04
Mars Aerobraking	2.05E-07	8.90E-05	8.92E-05
Mars Orbit	1.33E-06	5.78E-04	5.79E-04
Mars to Earth Insert	2.74E-09	1.19E-06	1.19E-06
Mars to Earth Transit	1.20E-06	5.01E-04	5.03E-04
EEV Entry (OD only)	1.15E-06	4.09E-06	5.14E-06
"worst" case attitude			**2.80E-03**
Total	**5.21E-06**	**1.73E-03**	**1.73E-03**
"best" case attitude			**6.33E-04**
Requirement	**---**	**---**	**4.00E-07**

The important take-away from Table 5-7 is that the probability of failure of the TPS due to MMOD impact exceeds the 4×10^{-7} reliability allocation. But it is also significant that the probability of failure due to orbital debris impact during Earth entry is larger than the allocation. This is problematic because the TPS is not shadowed/shielded by the orbiter following

separation. Separation times for prior spacecraft sample return canisters were approximately 4 hours for Genesis and Stardust and approximately 3 hrs for Hayabusa. In the case of Genesis, separation occurred outside of geosynchronous orbit and hence outside of the Earth orbital debris belt. If the EEV trajectory is similar, then the EEV will traverse the entire Earth orbital debris belt without the protection of the orbiter. If separation could be deferred to a later time, then the orbiter could provide more protection. The Apollo CSM separation occurred about 20 minutes before Earth interface. If the Genesis/SRC separation was deferred to 20 minutes before Earth interface, then separation would have occurred around 7,000 km. According to Figure 4-10, this would reduce the total fluence of 1 mm particles by a 1/3, which would help.

Another take-away from Table 5-7 is that the probability of failure due to perforation of the aft TPS is 330 times larger than the probability of failure of the forward TPS. This is a consequence of the forward and aft TPS ballistic limit equations. The size meteoroid that penetrates the aft TPS at 7 km/s and normal incidence is 0.847 mm and the size meteoroid that penetrates the forward TPS at 7 km/s is 5.56 mm. Substituting the 0.847 mm diameter into the meteoroid flux equation results in a flux 1,930 times larger than the flux of 5.56 mm diameter meteoroids, so it's not surprising that there is a much greater probability of aft TPS failure than forward TPS failure.

The line labeled "worst" case attitude in Table 5-8 is the attitude from Table 4-4 that produced the largest probability of TPS failure. The line labeled Total is the average of probability of TPS failure over the 24 attitudes listed in Table 4-4. This is representative of the probability of TPS failure for a randomly oriented EEV. The line labeled "best case attitude from Table 4-4 is the attitude that produced the smallest probability of TPS failure.

A bar chart similar to Figure 5-3 can be constructed for the mean number of penetrations (which is approximately equal to the probability of failure). The result is shown in Figure 5-4 the bar chart illustrates that the aft TPS is failing the requirement by 3 orders of magnitude.

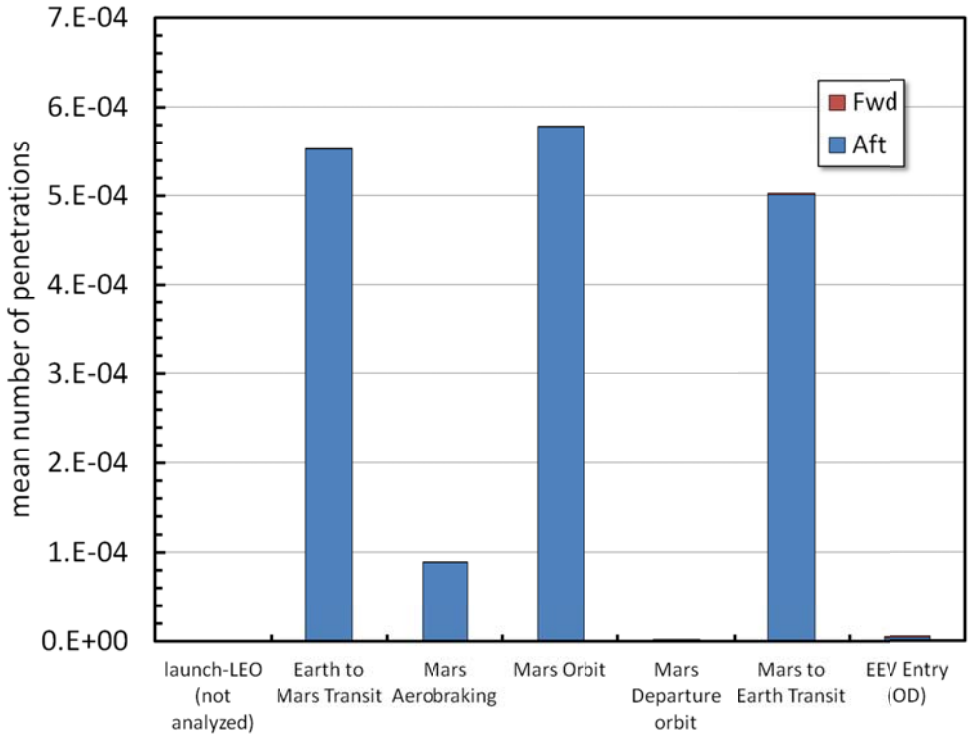

Figure 5-4 Mean Number of TPS Penetrations as Function of Mission Phase.

5.3 MMOD Shield Concept

The results for the MSR EEV MMOD shield concept PNP study are shown in Table 5-8. The results are broken out for each mission phase as well as for the two MSR EEV TPS components (aft and forward) and the conceptual MMOD shield.

Table 5-8. MSR EEV Analysis - MMOD Shield Concept Probability of TPS Failure due to MMOD Impact.

MSR EEV MMOD Shield Concept Results				
	Number of Perforations			
Missions Phase	**Forward**	**Aft**	**MMOD Shield**	**Total**
Launch-LEO (not analyzed)		…	…	…
Earth to Mars Transit	0.00E+00	0.00E+00	8.01E-08	8.01E-08
Mars Aerobraking	0.00E+00	0.00E+00	1.43E-08	1.43E-08
Mars Orbit	0.00E+00	0.00E+00	9.44E-08	9.44E-08
Mars to Earth Insert	0.00E+00	0.00E+00	1.97E-10	1.97E-10
Mars to Earth Transit	0.00E+00	0.00E+00	7.50E-08	7.50E-08
EEV Entry (OD only)	1.15E-06	4.09E-06	0.00E+00	5.24E-06
"worst" case attitude				**5.54E-06**
Total	**1.15E-06**	**4.09E-06**	**2.64E-07**	**5.50E-06**
"best" case attitude				**5.46E-06**
Requirement	**---**	**---**	**---**	**4.00E-07**

The analysis was performed assuming that the probability of TPS failure given an MMOD shield perforation was one. This is a conservative assumption. The assumption is necessary because testing is required to determine the extent of TPS damage given an MMOD shield perforation.

Table 5-8 shows that the MMOD shield has reduced the risk of TPS damage due to meteoroid impact to 2.64×10^{-7}, which is below the 4×10^{-7} requirement. However, the possibility of orbital debris impact occurs after the EEV is released from the orbiter and the EEV is no longer protected by the MMOD shield. Thus the risk of TPS failure due to orbital debris impact is unchanged from the unshielded cased, section 5.2. This short 2 hour exposure to the orbital debris environment is sufficient to cause the EEV to fail its probability of TPS damage due to MMOD impact by a wide margin.

Contours of numbers of TPS failures per square meter per exposure duration times 100 are plotted in Figure 5-5 for the orbital debris impacts during Earth entry phase. The EEV velocity vector is in the XZ plane of the figure and is pointing out the apex of the forward TPS cone. The contours of number of TPS failures are concentrated on the starboard side of the EEV due to the assumed argument of perigee of the orbit. The "hot" spot on the aft TPS will appear in a different location on the energy-absorbing sphere with different arguments of perigee.

The contouring levels preclude seeing the impact contours on the forward TPS because the number of impacts on the forward TPS are a ¼ of the number of impacts on the aft TPS.

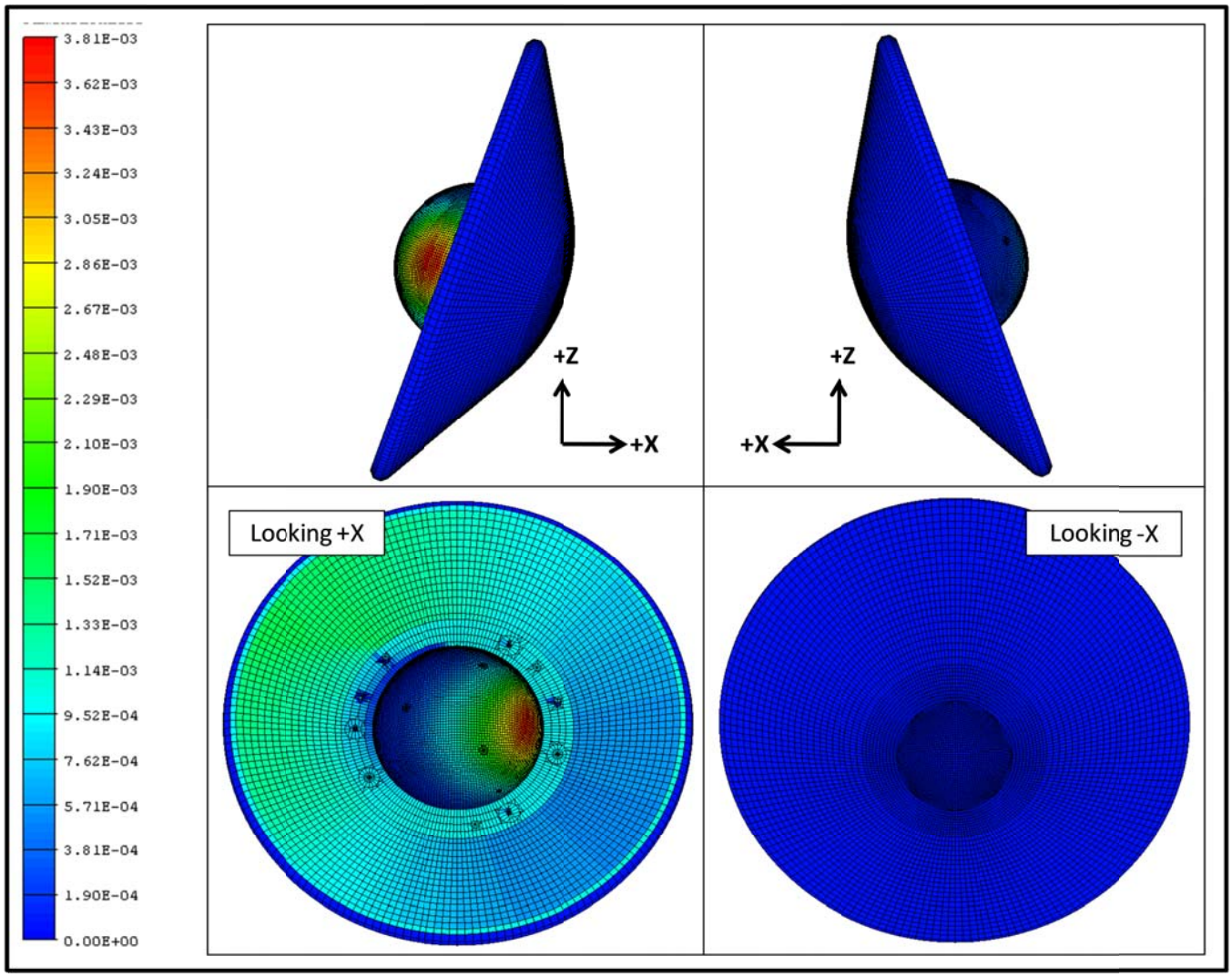

Figure 5-5. MSR EEV Analysis – MSR EEV Risk Contour Plot for Earth Reentry Phase

6. Conclusions

The MSR EEV MMOD analysis has shown that the currently designed MSR EEV thermal protection system does not meet the 4×10^{-7} maximum allowable risk requirement, given the assumptions made in this report. The aft TPS is made of SLA561V and fails the requirement by a factor of 4,300. The small density and strength of SLA561V makes an MMOD shield a necessity to meet the stringent 4×10^{-7} probability of TPS failure requirement. The forward TPS is made of carbon phenolic which is robust to MMOD impact, however, it too fails the requirement, but by the smaller factor of 13.

The assumption that perforation of the TPS down to the base structure leads to loss of specimen containment needs to be confirmed by TPS designers. The Orion program assumes smaller depths of penetration into the TPS results in loss of vehicle, so complete penetration of the TPS is likely an optimistic assumption. The Orion program TPS designers provided a map of allowable TPS penetration depths based on thermal allowable of the tile bond lines. Something similar is needed for EEV.

Surprisingly, the orbital debris impacts during entry was about 22% of the forward TPS risk of failure. This number may be an overestimate due to the conservative extrapolation of the orbital debris environment from 2,000 km to geosynchronous orbit made by Bjorkman. It may be possible to eliminate this conservatism by tasking the Orbital Debris Program Office with modifying their ORDEM 3.0 orbital debris environment to analyze the EEV Earth entry trajectory. ORDEM 3.0 does not require an extrapolation above 2,000 km altitude and greater confidence could be attached to the results.

Finally, hypervelocity impact tests of the actual EEV TPS materials are recommended. If it is desired to optimize the weight of the MMOD shield for the EEV, then testing to determine the conditions leading to unacceptable TPS damage following perforation of the shield is needed.

6.1 Forward Work Summary

The following summarizes forward work needed to reduce uncertainty in the MMOD risk assessment.

- MMOD requirements – need to confirm and/or update the 4×10^{-7} maximum risk value used in this assessment.
- Spacecraft TPS – thickness and material type for the EEV TPS need to be confirmed and/or updated in the next MMOD assessment.
- TPS failure criteria – need further efforts to define TPS failure criteria (damage limits for reentry). This will likely require tests (impact followed by arc-jet) and modeling of heating surrounding TPS cavities during reentry.
- Assessment inputs – need to include analysis of meteoroid and orbital debris impacts during initial launch/LEO phase, and meteoroids during reentry phase. Even though the MMOD risk during these mission phases is believed to be small relative to other mission phases, it should be quantified. Need to update the analysis using ORDEM 3.0 after it is released (no earlier than end of 2011).
- Ballistic limit equations – additional tests and simulations should be considered to reduce uncertainty in the ballistic limit equations used in this analysis, particularly TPS response at impact velocities greater than 7 km/s. The ballistic limit equations for the aft TPS need to be reviewed and updated based on additional hypervelocity impact tests.
- Optimize MMOD shielding/bioshield cover – evaluate additional shielding concepts to reduce mass and improve survivability. Evaluate risk as a function of when the MMOD shield is separated from the EEV at the end of mission.
- Quantify uncertainty – assess uncertainty in risk assessment results using MEM 1-sigma files.
- Other items described throughout the report and mentioned in conclusions that should be done to reduce uncertainty.

7. References

Anon., Progress Report No. 12, Hypervelocity Kill Mechanisms Program, NRL Report 6011, Naval Research laboratory, Washington DC, August 1963, AD389659, Page B6.

Boeder, P., "Space Station Program Natural Environment Definition for Design", *SSP 30425 Revision B.* Houston: NASA, 1994.

Bohl, William, "Project Orion OFT-1 MMOD Assessment Report", LM-ORN-0358, Lockheed-Martin Space System Co., Denver, CO, June 6, 2011.

Christiansen, E.L., "Design and Performance Equations for Advanced Meteoroid and Debris Shields", Int. J. Impact Eng., 14:145–156, 1993.

Cooke, William J., Re: Mars Sample Return Earth Entry Vehicle (MSREEV) meteoroid environment task. Email dated June 24, 2011 from William J. Cooke to Eric L. Christiansen, with enclosure entitled, "Meteoroid Environment Description for Mars Sample Return Earth Entry Vehicle (MSREEV)".

Gabriel A. Sanchez to Eric L. Christiansen titled "Return of SLA-561V Ablator Samples to Lockheed Martin", dated January 23, 1996

Liou, J.C.; M. Matney; P. Anz-Meador; D. Kessler; M. Jansen; J. Theall.; "The New NASA Orbital Debris Engineering Model ORDEM2000", *NASA/TP—2002-210780.* Houston: NASA, 2002.

Gershman, R.; Adams, M.; Dillman, R.; Fragola, J.; "Planetary protection technology for Mars Sample Return", *Aerospace Conference, 2005 IEEE, pp. 996- 1005*. 5-12 March 2005.

Halperson, S.M. Summary Report: Continuation of Experimental Study of Small Particle Impacts into Ablative Materials. NRL Memorandum Report 1927. Naval Research laboratory, Washington DC, July 1968. AD394828

Hedman, T, Hypervelocity Impact Test Plan for Orion Launch Abort System Structural Support Pad, version 4, Hypervelocity Impact Technology Group, Johnson Space Center, Houston, TX, June 14, 2010.

Lyons, Frankel, "Super-Light Ablator (SLA) Hypervelocity Impact Testing", *JSC 63789*, Johnson Space Center, Houston, TX, April 2007.

McNamara, H, Suggs, R., Kauffman, B., Jones, J., Cooke, W., and Smith, S. Meteoroid Engineering Model (MEM): A meteoroid model for the inner solar system. *Earth, Moon, and Planets* (2004) 95: 123-139. DOI 10.1007/s11038-004-9044-8.

Mattingly, R.; May, L.; "Mars Sample Return as a campaign," *Aerospace Conference, 2011 IEEE, pp.1-13*. 5-12 March 2011.

Ryan, S. and Christiansen, E.L., "Micrometeoroid and Orbital Debris (MMOD) Shield Ballistic Limit Analysis Program", NASA/TM–2009–214789, 2010

Taylor, A.; McBride, *N., A Radiant-Resolved Meteoroid Model*, Second European Conference on Space Debris, Organised by ESA, held 17-19 March, 1997, ESOC, Darmstadt, Germany (1997), ESA-SP 393., p. 375

8. Appendix A – MSR EEV MMOD Impact Risk Analysis Statement of Work

Statement of Work
Analysis of Micrometeorite (MM) impact on the Mars Sample Return Earth Entry Vehicle (MSREEV)

An agreement between NASA Ames Research Center
March 7, 2011

JSC POC: Eric Christiansen/ ARC POC: Ethiraj Venkatatpathy

Information to be provided by NASA Ames:

1. Approximate MSR mission concept.
    a. Launch Date of the spacecraft delivering the MSREEV to Mars
    b. Arrival date of the MSREEV and its orbit and duration in orbit at Mars
    c. Departure date from Mars and the Date of Earth Entry
    d. Drawing of the MSREEV as conceived in the ~ 2000 time frame
    e. No information is currently available for the spacecraft that will deliver the MRSEEV to Mars nor that on which it will be returned
    to the Earth

2. MSR EEV Cross Section with Materials lay-up

Analysis to be provided by NASA JSC in a written report:

1. Description of the MM distributions for the MSR missions and bounds on them
    a. MMOD in Low Earth Orbit (LEO) on way to Mars
    b. MM for transit to Mars
    c. MM during Mars Orbit
    d. MM during transit to Earth from Mars
    e. MMOD distribution in LEO upon return from Mars

2. Probabilities of hypervelocity impact as a function of velocity and particle sizes for the dwell times in each mission phase and the entire mission.

    a. Transit through LEO
    b. Transit from LEO to Mars Orbit
    c. While in Mars Orbit
    d. Transit from Mars to Earth
    e. Transit through LEO to Earth's surface
    f. Integrated probability of MMOD impact as a function of velocity and particle size for the entire mission.

3. Discussion of how the results of the analysis would change for missions of similar definition for later implementation (shifts on 26 month cycles)

4. Discussion of MMOD impact testing on Carbon Phenolic and 2D carbon-Carbon from prior HVI testing.

5. Discussion of directional aspects of the MM and MMOD fluxes and how the MSREEV could be best oriented with respect to the transit spacecraft(s) to avoid penetration of the outer mold line.

Written report due 6 months after receipt of ISPT funds at JSC

Interim presentation of results at 4 months from authority to proceed.

9. Appendix B - JPL Horizons Genesis Spacecraft Trajectory File Header

```
*******************************************************************************
 Revised: Nov 19, 2004      Genesis (SRC) Spacecraft / (Earth)           -47900
                           http://genesismission.jpl.nasa.gov/

 Genesis Sample Return Cannister (SRC):
   Launched: Aug 8, 2001 12:13:40 p.m. EDT (Delta 2 rocket)

 The SRC release was a one-second duration event beginning at 8-Sep-2004
 11:54:11.5 CT. End of contact with the springs was to occur at 11:54:12.5 CT.
 At this time, object -47900 (Genesis Sample Return Capsule) separated from
 -47 (Genesis bus). Half an hour later, the bus was diverted to an ultimately
 heliocentric trajectory, available separately using ID -47.

 SRC atmospheric entry was Sep 8, 2004 15:52:47.6 UTC.

 The SRC failed to deploy the drogue/parafoil at entry +127 seconds as planned,
 instead tumbling ballistically through the Earth's atmosphere to impact in
 sandy soil at geodetic coordinates 40.1278 deg (lat), 246.4919 deg (long).

 SPACECRAFT TRAJECTORY (from JPL navigation team):
  Solution name                                  Span
  ---------------------------------------        --------------------------
  OD145                                          2004-Aug-09 to 2004-Sep-06
  OD154                                          2004-Sep-06 to 2004-Sep-08
*******************************************************************************




*******************************************************************************
Ephemeris / WWW_USER Mon Sep 12 12:09:52 2011 Pasadena, USA      / Horizons
*******************************************************************************
Target body name: Genesis (SRC) Spacecraft (-47900) {source: pfile_src_od154.nio}
Center body name: Earth (399)                       {source: DE405}
Center-site name: BODY CENTER
*******************************************************************************
Start time      : A.D. 2004-Sep-07 13:52:00.0000 CT
Stop  time      : A.D. 2004-Sep-08 15:52:00.0000 CT
Step-size       : 1 minutes
*******************************************************************************
Center geodetic : 0.00000000,0.00000000,0.0000000 {E-lon(deg),Lat(deg),Alt(km)}
Center cylindric: 0.00000000,0.00000000,0.0000000 {E-lon(deg),Dxy(km),Dz(km)}
Center radii    : 6378.1 x 6378.1 x 6356.8 km     {Equator, meridian, pole}
Output units    : KM-S
Output format   : 03
Reference frame : ICRF/J2000.0
Output type     : GEOMETRIC cartesian states
Coordinate systm: Earth Mean Equator and Equinox of Reference Epoch
-------------------------------------------------------------------------------

                                       .
                                       .
                                       .
*******************************************************************************
Coordinate system description:

  Earth Mean Equator and Equinox of Reference Epoch
```

```
    Reference epoch: J2000.0
    xy-plane: plane of the Earth's mean equator at the reference epoch
    x-axis  : out along ascending node of instantaneous plane of the Earth's
              orbit and the Earth's mean equator at the reference epoch
    z-axis  : along the Earth mean north pole at the reference epoch

Symbol meaning

    JDCT     Epoch Julian Date, Coordinate Time
      X      x-component of position vector (km)
      Y      y-component of position vector (km)
      Z      z-component of position vector (km)
      VX     x-component of velocity vector (km/sec)
      VY     y-component of velocity vector (km/sec)
      VZ     z-component of velocity vector (km/sec)
      LT     One-way down-leg Newtonian light-time (sec)
      RG     Range; distance from coordinate center (km)
      RR     Range-rate; radial velocity wrt coord. center (km/sec)

Geometric states/elements have no aberration corrections applied.

 Computations by ...
     Solar System Dynamics Group, Horizons On-Line Ephemeris System
     4800 Oak Grove Drive, Jet Propulsion Laboratory
     Pasadena, CA  91109   USA
     Information: http://ssd.jpl.nasa.gov/
     Connect    : telnet://ssd.jpl.nasa.gov:6775  (via browser)
                  telnet ssd.jpl.nasa.gov 6775    (via command-line)
     Author     : Jon.Giorgini@jpl.nasa.gov
*******************************************************************************
```

10. Appendix C - SLA561V Ablator Ballistic Limit Equation

Fortran code of the SLA561V ablator ballistic limit equation implemented in bumper:

```
!-----------------------------------------------------------------------
! SLA-561V penetration equation (based on 1 data point,
! nylon projectile, 70deg impact angle, 6km/s impact into
! 1.9cm thick SLA-561V bonded to honeycomb panel
! damage description indicated entry hole 2.4cm x 3cm in size,
! some SLA filled cells completely destroyed, others damaged,
! penetration to bondline assumed but may be less).
!
! Damage mode: Penetration into SLA-561V only (not into substrate)
!
! Source:
!  E.L.Christiansen, 13 Nov 2006.
!
! Coded By:
!  Tom Prior, Hamilton Sundstrand/ESCG, 13-NOV-2006
      SUBROUTINE SLA561V(diam,velm,angr,projden, &
     & ABLATOR_THICK,ABLATOR_DEPTH)
      REAL(KIND=4),INTENT(OUT) :: DIAM
      REAL(KIND=4),INTENT(IN) :: VELM,ANGR,PROJDEN
      REAL(KIND=4),INTENT(IN) :: ABLATOR_THICK,ABLATOR_DEPTH

      REAL(KIND=4) :: VNORM
      REAL*8 PDEPTH
!
!  CALCULATE CRITICAL PENETRATION DEPTH
!
      PDEPTH = ABLATOR_THICK * (ABLATOR_DEPTH/100.0)
!
!  Calculate the normal component of the velocity vector
!
      VNORM=VELM*COS(ANGR)
!
!  CALCULATE CRITICAL PROJECTILE DIAMETER IN CM
!
      DIAM=(PDEPTH/3.7/SQRT(PROJDEN)/VNORM**(2./3.))**(18./19.)
      END SUBROUTINE SLA561V
```

11. Appendix D – Carbon Phenolic Ablator Ballistic Limit Equation

```
!-----------------------------------------------------------------------
!> @brief Carbon Phenolic TPS BLE.
!! @details The equation was developed by Michael D. Bjorkman, JSC/ESCG.
!! The BLE derivation is documented in JSC-66287. It is based on 7 tests
!! performed at NRL with glass projectiles and 2 tests performed for JSC
!! using 2017-T4 projectiles.
!!   @param[out] diam projectile diameter in cm
!!   @param[in] velm impact speed in km/s
!!   @param[in] angr impact angle measured for the element normal in radians
!!     (0 to pi/2)
!!   @param[in] projden projectile mass density in g/cm^3
!!   @param[in] ablator_thick carbon phenolic ablator thickness in cm
!!   @param[in] ablator_depth fraction, in percent, of the ablator thicknss that
!!     when penetrated causes failure.
!! @section sec2 Change History:
!!   \li /AUG 8, 2011/ subroutine added by Michael D. Bjorkman
!-----------------------------------------------------------------------
      SUBROUTINE CarbonPhenolic(diam,velm,angr,projden, &
      & ABLATOR_THICK,ABLATOR_DEPTH)
       REAL(KIND=4),INTENT(OUT) :: DIAM
       REAL(KIND=4),INTENT(IN) :: VELM,ANGR,PROJDEN
       REAL(KIND=4),INTENT(IN) :: ABLATOR_THICK,ABLATOR_DEPTH

       REAL(KIND=4) :: VNORM
       REAL(KIND=8) :: PDEPTH
!
!  CALCULATE CRITICAL PENETRATION DEPTH
!
      PDEPTH = ABLATOR_THICK * (ABLATOR_DEPTH/100.0_DP)
!
!  Calculate the normal component of the velocity vector
!
      VNORM=VELM*COS(ANGR)
!
!  CALCULATE CRITICAL PROJECTILE DIAMETER IN CM
!

DIAM=(PDEPTH/0.60885_DP/SQRT(PROJDEN)/VNORM**(2.0_DP/3.0_DP))**(18.0_DP/19.0_DP)
      END SUBROUTINE CarbonPhenolic
```

12. Appendix E - MEM Coordinate System

Definition of the MEM coordinate system from the MEM help file.

COORDINATES

All information displayed in the output files is relative to the spacecraft in local spacecraft coordinates. The figure below illustrates the coordinate frame.

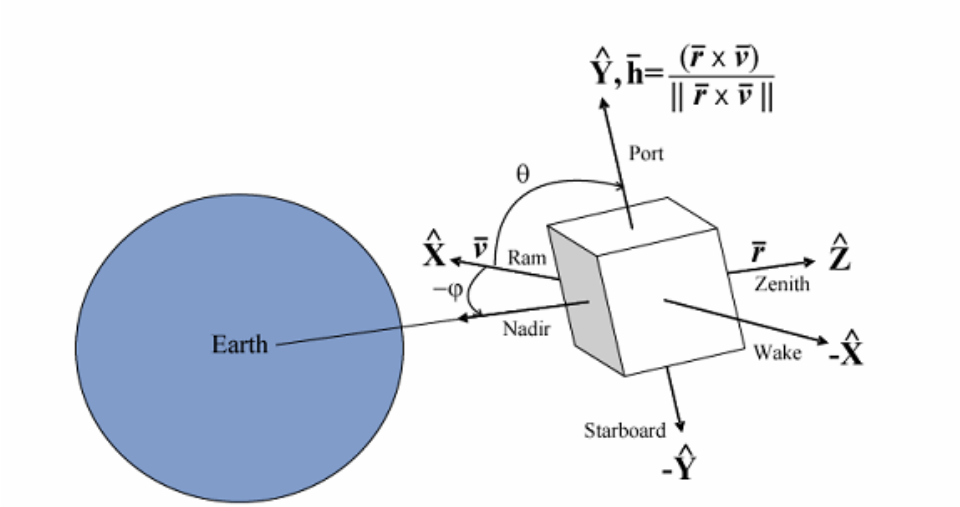

The spacecraft's velocity vector, $\bar{v}/\|\bar{v}\|$, defines the X unit direction. The Y unit direction is defined by the cross product of the position and velocity vectors, $(\bar{r} \times \bar{v})/\|\bar{r} \times \bar{v}\|$, or the angular momentum vector, $\bar{h}$. The Z unit direction is then defined by the cross product of the X and Y unit directions.

The elevation, φ, is measured from the spacecraft's velocity vector or X axis. Negative 90° points towards Earth or the nadir surface and positive 90° points towards space or the zenith surface, which is radially outward along the positive Z axis. The azimuth, θ, is measured positive counter clockwise from the velocity vector or X axis through the positive Y axis or port surface, in the XY plane. So 0° azimuth is the velocity vector, 90° azimuth is the port surface or positive Y axis and 180° azimuth is the wake surface or negative X axis.

For a circular orbit, the $\bar{r}$ and $\bar{v}$ vectors are perpendicular, but for elliptical orbits they are not and therefore the unit vectors for the body fixed frame must be defined as above. For circular orbits, the main output file will show similar if not exact fluxes and speeds for certain surfaces (Earth surface and nadir, etc.).

******NOTE****** *The meteoroid environment is directional and as the spacecraft changes directions relative to the Sun, the meteoroid directionality will change also. For Earth orbiting spacecraft additional shielding by the planet will block and unblock certain sources, making for rapid change in the directionality.*